

Electronic Theses and Dissertations, 2004-2019

2004

Development Of Titanium Nitride/molybdenum Disulphide Composite Tribological Coatings For Cryocoolers

Anil Pai
University of Central Florida

 Part of the [Materials Science and Engineering Commons](#)
Find similar works at: <https://stars.library.ucf.edu/etd>
University of Central Florida Libraries <http://library.ucf.edu>

This Masters Thesis (Open Access) is brought to you for free and open access by STARS. It has been accepted for inclusion in Electronic Theses and Dissertations, 2004-2019 by an authorized administrator of STARS. For more information, please contact STARS@ucf.edu.

STARS Citation

Pai, Anil, "Development Of Titanium Nitride/molybdenum Disulphide Composite Tribological Coatings For Cryocoolers" (2004). *Electronic Theses and Dissertations, 2004-2019*. 220.
<https://stars.library.ucf.edu/etd/220>

DEVELOPMENT OF TiN/MoS₂ COMPOSITE TRIBOLOGICAL COATINGS FOR
CRYOCOOLERS

by

ANIL U. PAI
B.S. Mumbai University, 1998

A thesis submitted in partial fulfillment of the requirements
for the degree of Master of Science
in the Department of Mechanical, Materials and Aerospace Engineering
in the College of Engineering and Computer Science
at the University of Central Florida
Orlando, Florida

Spring Term

2005

Major Professor: Neelkanth G. Dhere

© 2005 Anil U. Pai

ABSTRACT

Hydrogen is a clean and sustainable form of carrier of energy that can be used in mobile and stationary applications. At present hydrogen is produced mostly from fossil sources. Solar photoelectrochemical processes are being developed for hydrogen production. Storing hydrogen can be done in three main ways: in compressed form, liquid form and by chemical bonding. Near term spaceport operations are one of the prominent applications for usage of large quantities of liquid hydrogen as a cryogenic propellant. Efficient storage and transfer of liquid hydrogen is essential for reducing the launch costs. A Two Stage Reverse Turbo Brayton Cycle (RTBC) CryoCooler is being developed at University of Central Florida. The cryocooler will be used for storage and transport of hydrogen in spaceport and space vehicle application. One part in development of the cryocooler is to reduce the friction and wear between mating parts thus increasing its efficiency. Tribological coatings having extremely high hardness, ultra-low coefficient of friction, and high durability at temperatures lower than 60 K are being developed to reduce friction and wear between the mating parts of the cryocooler thus improving its efficiency.

Nitrides of high-melting-point metals (e.g. TiN, ZrN) and diamond-like-carbon (DLC) are potential candidates for cryogenic applications as these coatings have shown good friction behavior and wear resistance at cryogenic temperatures. These coatings are known to have coefficient of friction less than 0.1 at room temperature. However, cryogenic environment leads to increase in the coefficient of friction. It is expected that a composite consisting of a base layer of a hard coating covered with layer having an ultra-low coefficient of friction would provide better performance. Extremely hard and extremely low friction coatings of titanium nitride, molybdenum disulphide, TiN/MoS₂ bilayer coatings, DLC and DLC/MoS₂ bilayer coatings have been chosen for this application. TiN film was deposited by reactive DC magnetron sputtering system from a

titanium target and MoS₂ film was deposited by RF magnetron sputtering using a MoS₂ target. Microwave assisted chemical vapor deposition (MWCVD) technique was used for preparation of DLC coatings. These composite coatings contain a solid lubricating phase and a hard ceramic matrix phase as distinctly segregated phases. These are envisioned as having the desired combination of lubricity and structural integrity. Extremely hard coatings of TiN and DLC were chosen to provide good wear resistance and MoS₂ was chosen as the lubricating phase as it provides excellent solid lubricating properties due to its lamellar crystal structure.

This thesis presents preparation; characterization (SEM and XRD), microhardness and tribological measurements carried out on TiN and TiN/MoS₂ coatings on aluminum and glass substrate at room temperature. It also presents initial development in preparation of DLC coatings.

ACKNOWLEDGMENTS

First and foremost, I would like to take this opportunity to thank my advisor, Dr. Neelkanth G. Dhere, for his helps and support throughout this work. I enjoyed working under his supervision and appreciate his constant guidance and encouragement. It really was a great experience and an overall growth of personality. I would like to thank Dr. Jayant Kapat and Dr. Linan An for serving on my final examination committee and for their invaluable suggestions.

This research is supported by NASA Glenn Research Center through the NASA Hydrogen project for Florida Universities. I am also thankful Dr. A. Kumar, Dr. A. Sikder and Parshuram at University of South Florida for helping with the ball-on-disc friction measurements, to Dr. R. Vaidyanathan and colleagues at University of Central Florida for helping with the microhardness measurements, and to Dr. Quanfeng Chen and colleagues for friction measurements at UCF.

I would like to acknowledge the help of following colleagues during this project: Anant Jahagirdar, Ankur Kadam, Vivek Gade, Sachin Kulkarni, Sachin Bet, Vinaykumar Hadagali, Upendra Avachat, Jyoti Shirolkar and others at the Florida Solar Energy Center.

Words cannot truly express my deepest gratitude and appreciation to my parents, brother and family members, who always gave me their love and emotional support.

TABLE OF CONTENTS

LIST OF FIGURES	ix
LIST OF TABLES	xi
INTRODUCTION	1
Preparation and Properties of Tribological Thin Coatings.....	2
Coating Damage in Tribology.....	7
Damage without Exchange of Material	7
Damage with Loss of Material, i.e. Wear.....	7
Damage with Material Pick Up	8
Substrate Properties.....	8
Hardness	8
Surface Roughness	8
Corrosion Resistance	9
Material Homogeneity.....	9
Coating Properties.....	10
Thickness.....	10
Topography.....	11
Adhesion.....	11
Mechanical Properties	11
Residual Stress.....	12
Toughness.....	13
Hardness	13

Effect of Microstructure on Hardness.....	14
Grain Size and Grain Boundary Structure	14
Metastable Structures	15
Impurities	15
Film Texture.....	15
Basic Mechanisms of Friction and Wear of Coatings.....	16
Main Mechanical Factors influencing Tribological Behavior.....	16
Wear Mechanisms	17
Adhesive/Sliding Wear.....	17
Abrasive Wear	21
Fatigue Wear.....	21
Fretting Wear	21
Delamination Wear	22
Oxidation Wear.....	22
Transfer Films	22
Application-oriented Optimization of Tribological Coatings	23
Application of Tribological Coatings to the Two Stage Reverse Turbo Brayton Cycle (RTBC) Cryocooler.....	24
EXPERIMENTAL TECHNIQUES.....	27
Substrate Preparation	28
Sputtering Chamber for Deposition - TiN and MoS ₂ Film.....	29
Series of Deposition of TiN Layer	30

Series-1 - TiN Film.....	30
Series-2 - TiN Film.....	31
Series-3 - TiN Film.....	31
Deposition of MoS ₂ Film	31
Deposition of TiN/MoS ₂ Film.....	35
RESULTS AND DISCUSSION.....	38
Series-1 TiN Film Results and Discussion.....	38
Series-2 TiN Film Results and Discussion.....	38
Series-3 TiN Film Results and Discussion.....	42
Results and Discussion - MoS ₂ Film.....	52
Results and Discussion – TiN/MoS ₂ Film	54
DIAMOND-LIKE CARBON FILM.....	70
Introduction.....	70
Experimental Technique	73
Results and Discussion.....	76
CONCLUSIONS.....	79
REFERENCES	81

LIST OF FIGURES

Figure 1: Tribology System	18
Figure 2: Sputtering Chamber.....	29
Figure 3: Bumps on Si-wafer and Sliding Action.....	36
Figure 4: Mask Design.....	36
Figure 5: XRD Patterns of Series-2 - TiN (Sr2-Sp 1 and Sr2-Sp 4) with (111) peak orientation.	41
Figure 6: Scanning Electron Microscopy Image Series-3 - TiN (Sr3-Sp 3).....	45
Figure 7: XRD Pattern of Series-3 - TiN (Sr3-Sp 3)	45
Figure 8: Loading-unloading Curve for TiN samples of Series-3 - TiN (Sr3-Sp 3).....	46
Figure 9: TEM Cross-section showing Glass/Ti/TiN/Pt Layer	46
Figure 10: Interface - Glass to Ti Layer at Magnification of 130K.....	47
Figure 11: Interface - Ti Layer to TiN layer at Magnification of 390K	47
Figure 12: Friction Tests of TiN Sample (Sr3-Sp4) with Steel Ball and TiN Coated Ball	51
Figure 13: Wear Tests of TiN Sample (Sr3-Sp4) with Steel Ball and TiN Coated Ball	51
Figure 14: TiN Coating on Aluminum Substrate and inside of Aluminum Ring.....	51
Figure 15: Scanning Electron Microscopy Image of MoS ₂ Coating	53
Figure 16: XRD Pattern of MoS ₂ Film	53
Figure 17: XRD Pattern of TiN/MoS ₂ Film (Samp. 2).....	56
Figure 18: Interface – Glass to Ti Layer.....	56
Figure 19: Interface – Glass to Ti Layer at Magnification of 390K.....	57
Figure 20: Grains in Ti Layer at Magnification of 49K.....	57
Figure 21: Grains in TiN Layer at Magnification of 49K.....	58

Figure 22: Interface - Ti Layer to TiN Layer at Magnification of 98K	58
Figure 23: Interface - TiN Layer to MoS ₂ Layer at Magnification of 115K	59
Figure 24: Interface - TiN Layer to MoS ₂ Layer at Magnification of 390K	59
Figure 25: Optical Microscopy Image of TiN/MoS ₂ Film on Bumps on Si-wafer	61
Figure 26: Friction Test of TiN/MoS ₂ Sample (Samp. 2 dep. Conditions) on Si-wafer.....	61
Figure 27: Friction Test of TiN/MoS ₂ Samples with Steel Ball	65
Figure 28: Friction Test of TiN/MoS ₂ Samples with TiN Coated Steel Ball	65
Figure 29: Friction Test of TiN/MoS ₂ Samples with TiN/MoS ₂ Coated Steel Ball	66
Figure 30: Wear Test of TiN/MoS ₂ Samples with Steel Ball	68
Figure 31: Wear Test of TiN/MoS ₂ Samples with TiN Coated Steel Ball.....	68
Figure 32: Wear Test of TiN/MoS ₂ Samples with TiN/MoS ₂ Coated Steel Ball	69
Figure 33: Microwave CVD Setup	75

LIST OF TABLES

Table 1: Mechanical and Tribological Properties of Commercially Available Hard Coatings.....	4
Table 2: Mechanical and Tribological Properties of MoS ₂ , Diamond, and Different DLC Films..	6
Table 3: Deposition Parameters of Series-1 TiN Samples.....	33
Table 4: Deposition Parameters of Series-2 TiN Samples.....	33
Table 5: Deposition Parameters of Series-3 TiN Samples.....	34
Table 6: Deposition Parameters of TiN/MoS ₂ Samples	37
Table 7: Series 2 - EDS Analysis and Results of Microhardness Measurement.....	39
Table 8: Hardness Values for Series-3 TiN Sample (Sr3-Sp3)	48
Table 9: Summary of Friction Tests by Ball-on-disc and Pin-on-disc Method on Series-3 TiN Films	50
Table 10: Summary of Wear Tests by Pin-on-disc Method on Series-3 TiN Films.....	50
Table 11: Summary of Friction Tests by Ball-on-disc and Pin-on-disc Method on Series-3 TiN Films.....	60
Table 12: Summary of Friction Tests	64
Table 13: Summary of Wear Tests	67

INTRODUCTION

Tribology is the branch of science and technology concerned with contacting surfaces having a relative motion against each other. It deals with the phenomena of friction and wear of surfaces with and also without lubrication. Therefore, interactions between solid surfaces as well as between solid surfaces and liquids and gases have to be considered.

One way to reduce friction and wear is to use lubricants; another way is to modify the surfaces by deposition of coatings or by special surface treatments. The latter means that the near-surface regions will be modified, e.g., by a plasma process or by ion implantation. In many practical cases both coatings and lubricants are used. The coatings help in reducing the amount of lubricants needed and improve the behavior of mechanical components under insufficient lubrication conditions. These tribological coatings also allow the use of markedly cheaper bulk materials for the moving components.

These coatings add physical properties such as lubricity, hardness or corrosion resistance, to lower-value substrates that improve the overall quality of the component. In addition the substrate can be designed for strength and toughness to avoid catastrophic failure of the component. Both the coating and substrate properties should be optimized taking into account mechanical, structural, chemical, electrical, thermal and dimensional properties [1].

Friction and wear are not intrinsic properties of a material; they are functions of the tribological system. A tribological system is composed of three basic elements,

- the structure - the types of materials in contact and the contact geometry,
- the operating conditions - the gross motion, loads, stresses, and duration of operation, and

- the environment and surface conditions - including the surface environment and chemistry, surface topography, and ambient temperature.

The sheer number of factors affecting performance makes fundamental studies exceedingly difficult. It is not possible to predict the optimum coating for a given application only from theoretical considerations. The basis of selection is to a large extent the experience of experts [2]. In the context of tribology, we define thin films where the effect of the substrate on the system properties cannot be neglected.

A large number of tribological coatings are known. Gold-colored titanium nitride (TiN) or titanium aluminum nitride (TiAlN) are widely established as hard coatings for cutting tools. Molybdenum disulfide (MoS₂) with an extremely low friction coefficient under vacuum conditions is a preferred material for space applications [2].

Preparation and Properties of Tribological Thin Coatings

A large variety of thin-film materials and preparation methods are known. A general distinction and classification of these methods can be found in the literature [3-4]. For thin-film depositions the following three groups can be distinguished [3].

- gaseous-state processes: chemical vapor deposition (CVD), physical vapor deposition (PVD), ion beam-assisted deposition (IBAD);
- solution-state processes: electrochemical deposition, sol-gel processes, chemical solution processes; and
- molten- or semimolten-state processes: thermal and plasma spraying, laser treatment, welding.

For tribological applications, well adhering, hard, and wear-resistant thin films, in many cases additionally with low friction coefficients are demanded. For this type of coating the

gaseous-state processes have the best potential. A higher film quality can be achieved by the plasma- or ion-assisted variants of these methods. In these cases the simultaneous bombardment of the growing film with ions improves several properties markedly. The additional ion bombardment of the films causes several modifications of the film–substrate system that are very important for tribological applications, for example:

- lower substrate temperatures;
- homogeneous and dense films;
- high hardness, Young's modulus, and wear resistance;
- extremely smooth film surfaces; and
- improved film adhesion.

However, ion bombardment can cause high compressive stress in a film and therefore it can lead to deterioration of the adhesion.

Some properties of hard and wear-resistant coatings mainly used for wear reduction of tools are summarized in Table 1 [2]. These coatings are commercially available. For the deposition of high-quality, well-adhering coatings, for the PVD and CVD and Plasma Enhanced CVD techniques, an additional heating of the substrates to temperatures between about 400 °C and 1000 °C is necessary. The substrate temperature, expressed, for example, in relative units as the ratio of substrate temperature T_S and melting temperature T_M , can markedly influence the film structure [5].

Table 1: Mechanical and tribological properties of commercially available hard coatings.

	TiN	TiCN	TiC	TiAlN	CrN	Al ₂ O ₃
Deposition method	PVD/CVD	PVD/CVD	CVD	PVD	PVD/CVD	CVD/PVD
Typical thickness (μm)	1–5	1–5	1–5	1–5	1–15	1–5
Hardness (HV 0.05) ^(a)	2300	3000	3100	3000	1900	2100 (HV 0.1)
Oxidation temperature (°C) ^(b)	>450	>350	>350	>700	>600	
Friction coefficient ^(c)	0.5–0.7	0.5–0.7	0.5–0.7	0.6–0.8	0.5–0.8	0.7–0.9
Abrasive wear resistance	++	+++	+++	+++	++	++
Adhesive wear resistance against steel	++	+ / +++	+	++	++	+++
Resistance against wear by diffusion	++	+	+	+++	++	+++
Corrosion protection of base material ^(d)	+	+	+	+	++	+

^(a) Mean hardness from literature values may vary by 10% owing to variations of chemical composition, thickness, and residual stresses.

^(b) Oxidation temperature designates the temperature at which oxidation of the coatings results in significant deviation of coating properties.

^(c) Tests against ball-bearing steel (ball-on-disk, 1 N normal load, nonlubricated, ambient atmosphere)—values after reaching equilibrium state, characterized by intensive material transfer from steel to coating. Before material transfer dominates, low values in the region of 0.2 were measured. The value of steel against steel is 0.6–0.9.

^(d) These coatings do not corrode themselves, building up a barrier for the base material. In the case of pinholes in the coatings local galvanic elements may be formed leading to pitting corrosion.

Applications where very low friction coefficients are needed, other films like DLC in different modifications or molybdenum and tungsten sulfide (MoS_2 , WS_2) can be chosen. Such solid lubricant films commonly are classified as soft or hard. Soft films (hardness < 10 GPa) are those with lamellar structure like MoS_2 , WS_2 , MoSe_2 , or graphite, but also polymer fluorides and soft metals. Examples of hard solid lubricant films are DLC in different modifications, some oxides, carbides, or borides [6].

Important properties of different types of diamond, DLC, and MoS_2 films are summarized in Table 2 [2]. Especially, Si-DLC is found to exhibit clearly lower friction coefficients than other types of DLC. Sulfide as well as DLC and ta-C films can be deposited on unheated substrates. However, typical substrate temperatures for diamond film deposition lie in the range 700–1000 °C [2].

Table 2: Mechanical and tribological properties of MoS₂, diamond, and different DLC films.

	MoS₂	Me-DLC	DLC	Si-DLC	ta-C	Diamond
Deposition method	PVD	PVD	PECVD	PECVD	PVD	CVD
Thickness (μm)	0.1–1	1–5	1–5	1–5	1–3	3–10
Hardness (HV 0.05) ^(a)	<500	800–1800	1500–3500	600–1000	3000–7000	10000
Typical values for compressive stress (GPa)		0.1–1	1–3	1	2–6	
Temperature of transformation (°C) ^(b)	350	350	400	500	450	>600
Friction coefficient ^(c)	0.02–0.1	<0.2	0.15–0.2	0.07–0.15	0.15–0.2	< 0.2
Abrasive wear resistance		+	+++	+	++++	++++
Adhesive wear resistance against steel		++	+++	++	+++	(+++) only with good cooling
Corrosion protection of base material ^(d)		+	+++	+++	+++	+++

^(a) Mean hardness from literature, values may vary by 10% owing to variations of chemical composition, thickness, and residual stresses.

^(b) Transformation temperature designates the temperature at which oxidation and/or structural and/or chemical changes of the coatings results in significant deviation of coating properties. The exact nature of these processes is not known.

^(c) Tests against ball-bearing steel (ball-on-disk, nonlubricated, 1 N normal load, ambient atmosphere)—values after reaching equilibrium state. The value of steel against steel is 0.6–0.9.

^(d) These coatings do not corrode by themselves, building up a barrier for the base material. In the case of pinholes in the coatings local galvanic elements may be formed leading to pitting corrosion.

Coating Damage in Tribology

A tribological coating can fail prematurely due to detachment, delamination, cracking and/or spalling of the coating material. Similar damage mechanisms rarely occur for homogeneous materials. On the other hand, the typical mechanisms for gradual wear are the same for coatings as for homogeneous materials. A classification of these mechanisms into three categories is described below [7].

Damage without Exchange of Material

This category basically involves permanent changes in component geometry and/or in surface topography. Decisive parameters for a change in geometry are Young's modulus and hardness of coating and substrate, and coating toughness. Coating hardness is the crucial parameter for scratch resistance, and coating toughness or fracture resistance for the resistance to surface cracking.

Damage with Loss of Material, i.e. Wear

The wear resistance of a coated component is mainly determined by the coating as long as it covers the contact area. As soon as the coating is partly worn through, or the substrate is exposed due to adhesive failure or cracking and spalling, the wear resistance of the substrate material becomes important. An in-depth description of the large number of wear mechanisms found in the applications of coated components is given in [3]. However, two main categories can be distinguished: wear dominated by coating detachment and wear caused by gradual removal of coating material. The latter often involves mild wear due to abrasion, erosion, chemical

dissolution, etc., and does not deviate from the mechanisms causing wear of homogeneous materials.

Damage with Material Pick Up

Work material locally adhered to e.g. the surface of a sheet forming tool used in the automotive industry will inevitably produce indentations or scratches in the surface of the product. Material transfer between the contact surfaces of sliding machine elements is a similar problem often named galling, scuffing or seizure. Material pick up of material from the counter surface is; again, not unique to coating composites. It is generally reduced or avoided by giving the surface a smooth topography and making sure that the chemical affinity to the counter surface is low. The important properties of the substrate, the coating and the interface play significant roles and are listed below.

Substrate Properties

Hardness

The substrate hardness is of prime importance for the tribological application. If the thin coating is not supported sufficiently, it will fail at relatively low contact stresses as it cannot follow deformation of the substrate.

Surface Roughness

The surface roughness should be as low as practically achievable for two reasons

- Thin coatings often replicate the substrate surface and roughness peaks cause local stress intensities during service resulting in local failure of the coating, which in turn may destroy the rest of the coating by third body abrasion.
- Secondly, ion-assisted deposition processes generally produces compressive stresses in the coating. This may provoke coating delamination at roughness peaks in the same manner as occurs at macroscopic corners [1].

Corrosion Resistance

Thin surface coatings usually contain defects in the form of pinholes or grain boundary voids which may go through the whole coating thickness. In addition, a coating is often electrochemically more noble than the substrate surface [8]. As a result, the exposed substrate at the bottom of the pinholes is severely attacked and the rest of the coating fails at some later stage either due to removal of the supporting substrate material or by the formation of the voluminous corrosion products at the interface resulting in coating removal. It is therefore important that both coating and substrate should have good corrosion resistance properties if a component is used in corrosive environment.

Material Homogeneity

Coarse phase differences in substrate materials may lead to differential adhesion of the coating to different phases that may result in local failures. As well the sputter-cleaning step prior to coating may cause differential sputtering of the different phases thereby roughening the surface

[9]. A better dispersion of phases generally results in better corrosion resistance too. Therefore, the use of powder-metallurgical material grades may be a key factor in design of coated components.

In addition to the above-mentioned properties, electric and magnetic properties of the substrate strongly influence coating properties in deposition processes. For instance, magnetic substrates may interact with the magnetic field in a magnetron sputter PVD process. This results in varying coating properties [1]. Component shape may also play a key role during deposition process thereby influencing the coating properties.

Coating Properties

The deposition parameters (substrate temperature, plasma characteristics, substrate bias, etc.) together with the substrate characteristics (e.g. composition, microstructure, topography) determine the coating characteristics (thickness, chemical composition, microstructure, topography, etc.). The influence from substrate is primarily related to nucleation and growth of the coatings and to the coating topography. Consequently the substrate material and surface preparation is crucial to the coating topography and adhesion and in turn to the performance of coating composite.

Some of the relevant coating characteristics and basic properties involved in coatings development are described below

Thickness

Appropriate coating thicknesses play a significant role to obtain good tribological properties. Under rolling contact fatigue conditions, for example, it was unexpectedly found that

sub-micron coatings performed significantly better than thicker coatings [10]. For a given load and contact geometry, an appropriate choice of coating thickness may allow the maximum shear stresses to be developed at locations away from the coating-substrate interface [11].

Topography

There are several aspects on the optimum topography of thin hard coatings. To minimize the maximum contact stresses on the asperity level, the coating surface should be as smooth as possible. Since most thin coatings inherit the substrate topography, the final step in substrate surface preparation should be a careful polishing or a very mild blasting. This is also recommended to increase the practical adhesion of coatings with high residual stresses.

Adhesion

A key aspect of coatings is adhesion between the coating and substrate to assure good performance. Sufficient adhesion is generally achieved by appropriate surface pretreatment, cleaning, by using adhesion promoting interlayers, etc.

Mechanical Properties

Wear resistance of coating are usually conferred by their hardness. The Young's modulus of the coating (E_c) is important for measurements and calculations of the stress state in a coating and the cracking and delamination behavior of coating composites. For example, a low Young's modulus may result in less stringent demands on substrate load support compared with brittle

ceramic coatings [1]. The load and depth sensing indentation (DSI) instruments are generally used to measure the mechanical properties of thin surface coatings.

Residual Stress

Tribological PVD and CVD coatings usually display residual stresses (σ_{res}). Structural misfits in epitactic nucleation and growth, and ion bombardment during growth are two stress origins of intrinsic nature. The stresses induced during cooling from the deposition temperature due to mismatch in thermal expansion between coating and substrate materials, and possible phase transformations occurring during cooling are two sources of the external origin. The final stress state is a combination of these components [12-14]. The actual stress during application (σ) is given by

$$\sigma = (\sigma_{\text{res}} + \sigma_{\text{app}})$$

where (σ_{app}) denotes the stress field induced by the application, including external forces and thermal mismatch stresses due to frictional heating.

Coating internal stress may impair the performance of coated components in several ways. On the other hand, compressive stresses in coating may be desirable because they increase cohesion, fracture toughness, resistance to fatigue failure of the coating. Too high compressive stresses may result in spontaneous coating detachment, e.g. during cooling from the process temperature. In less severe cases, the coating may detach when the coated component becomes loaded externally. The risk for detachment is closely related to the geometry and topography of the coating/substrate interface, the smoother the interface the less is the risk. On an uneven surface, the

interfacial normal or shear stress generated by the residual coating stresses can exceed 50% of the residual stress level [12].

Toughness

Coating cracking or fracture often precedes damage of PVD and CVD coatings. Thus, the ability of the coating composite to accommodate deformation in tension or compression without crack nucleation and propagation is crucial. Since cracking is initiated by tensile stresses, any compressive residual stress has first to be relaxed. Consequently, if the coating initially has a high compressive residual stress, the coated component can take more tensile strain before the coating will fracture. The critical component strain is thus a more important parameter than the critical intrinsic tensile strain of the coating [12].

Hardness

Hardness is an important material property of concern in tribological coatings. The hardness of a material is usually defined as its resistance to plastic deformation. It affects wear resistance and plays an important role in the friction and lubrication of surface films in contact. It is a complex property related to strength of interatomic forces and apparently depends on more than one variable. Hard materials are generally modeled by a deep potential energy well with steep walls. These characteristics imply a combination of high cohesive energy and short bond length. Measures of cohesive energy are the heat of sublimation and enthalpy of compound formation. It is apparent that the hardest materials are covalently bonded, and that increasing the ionic character of

the bond leads to reduced hardness. At a microscopic level, directional bonds resist distortion and rupture more readily by concentrated loads than do ionic bonds.

Effect of Microstructure on Hardness

Grain Size and Grain Boundary Structure

In metal and alloy films the hardness correlates well with the Hall-Petch relation given by

$$H = H_i + K_H * l_g^{-1/2}$$

where H is the hardness, H_i is the intrinsic hardness of single crystal, l_g is the grain size and K_H is a material constant. However the above equation does not apply to refractory compound coatings because the hardness of fine-grained films is frequently close to bulk material value.

Apparently the hardness and strength of refractory compounds is the perfection of the grain boundaries. Porosity and fine microcracks are very harmful to such coatings and lower their strength and hardness significantly. Increasing the substrate temperature is the most common and simplest way to reduce the grain boundary defect structure and enhance the hardness of these compounds. Elevated temperatures promote the strengthening of grain boundary by eliminating void networks. The grain size increases as does hardness contrary to Hall-Petch equation however with further grain growth at still higher temperatures, the hardness drops and reaches bulk values [15].

Metastable Structures

Metastable phases are frequently observed in refractory compound films as high deposition rates and low substrate temperature are conducive to formation of nonequilibrium structures and fine grain size. Manifestations of the metastability are the incorporation of C and N in interstitial lattice sites and generation of supersaturated solid solutions. The incorporated interstitials tend to distort the lattice and subsequent difficulty in initiating dislocation motion is reflected in increased hardness. These coatings are highly stressed and have hardness values far above those for the corresponding equilibrium structures [15].

Impurities

Since hard PVD coatings are grown in medium vacuum or under higher pressure ambient, the incorporation of noble gases, C, N and O from residual gases and impurities from chamber hardware and walls is not uncommon. The deposit impurities are located in both substitutional, interstitial as well as grain boundary sites at total levels of few atomic percent. The mechanism of hardening due to impurities apparently involves the electrostatic attachment of the later to charged dislocations in ionic crystal and to dangling dislocation bonds in covalent compounds limiting dislocation mobility by pinning effects [15].

Film Texture

Isotropic behavior is usually observed in case of randomly oriented planes as compared to crystallographic planes oriented parallel to the film surface. Films grown by PVD and CVD techniques usually display a preferred orientation, however with low index planes lying parallel to

the substrate surface, creating a texture that is strongly dependent on virtually all deposition and process variables.

Basic Mechanisms of Friction and Wear of Coatings

The tribological properties of a given coating system do not depend only on the coating itself, but also on the surroundings, e.g., counter-surface, substrate material, gaseous or lubricated environment, generation of abrasive wear particles, etc. This means that they are not a property of the coating alone but a property of the whole system as shown in Figure 1 [2]. In order to understand the behavior of contacting surfaces it is a prerequisite to understand the whole tribological system.

Main Mechanical Factors Influencing Tribological Behavior

The main factors are:

- Hardness and elasticity of the contacting surfaces (mainly the substrates) determining the contact area at a given load.
- Hardness and wear resistance of the coating itself determine the degree of wear of the coating, if other factors such as substrate being too soft or a roughness being too high do not lead to coating failure.
- Roughness of the surfaces determines, to some extent, the degree of mechanical clamping of the surfaces. It also determines whether the surface carrying the coating can sustain the load. In that case, hard roughness asperities would be responsible for some degree of ploughing of the counter-surface.

- The friction between the surfaces is responsible for the introduction of shear stresses in the coating, the coating substrate interface, and the substrate and also for the degree of frictional heating and energy input into the contact zone.
- The speed of relative motion and the frequency at which certain areas of the contacting surfaces meet each other, e.g., in a bearing. This determines together with friction the degree of energy input per unit area and time and also the height of the energy flash during each contact event.
- Besides hardness, toughness of the surfaces determines the degree of wear particle generation and fatigue of the surface (pitting wear, fatigue of bearings).
- Chemomechanical effects, i.e., wear particle generation under high pressures and contact temperatures in an unfavorable, e.g., corrosive environment.

Wear Mechanisms

Wear may be defined as the progressive removal of material from surfaces that are under load in relative motion. Several different mechanisms have been identified to characterize contact wear and are described below

Adhesive/Sliding Wear

Adhesive wear occurs when applied tangential forces cause fracture between surfaces bonded at asperities. The fracture path can follow the original microweld interface. Other paths lie above or below the interface when the strength of the bonds between asperities exceeds the cohesive strength of the bodies in contact. The result is material transfer usually from the softer to

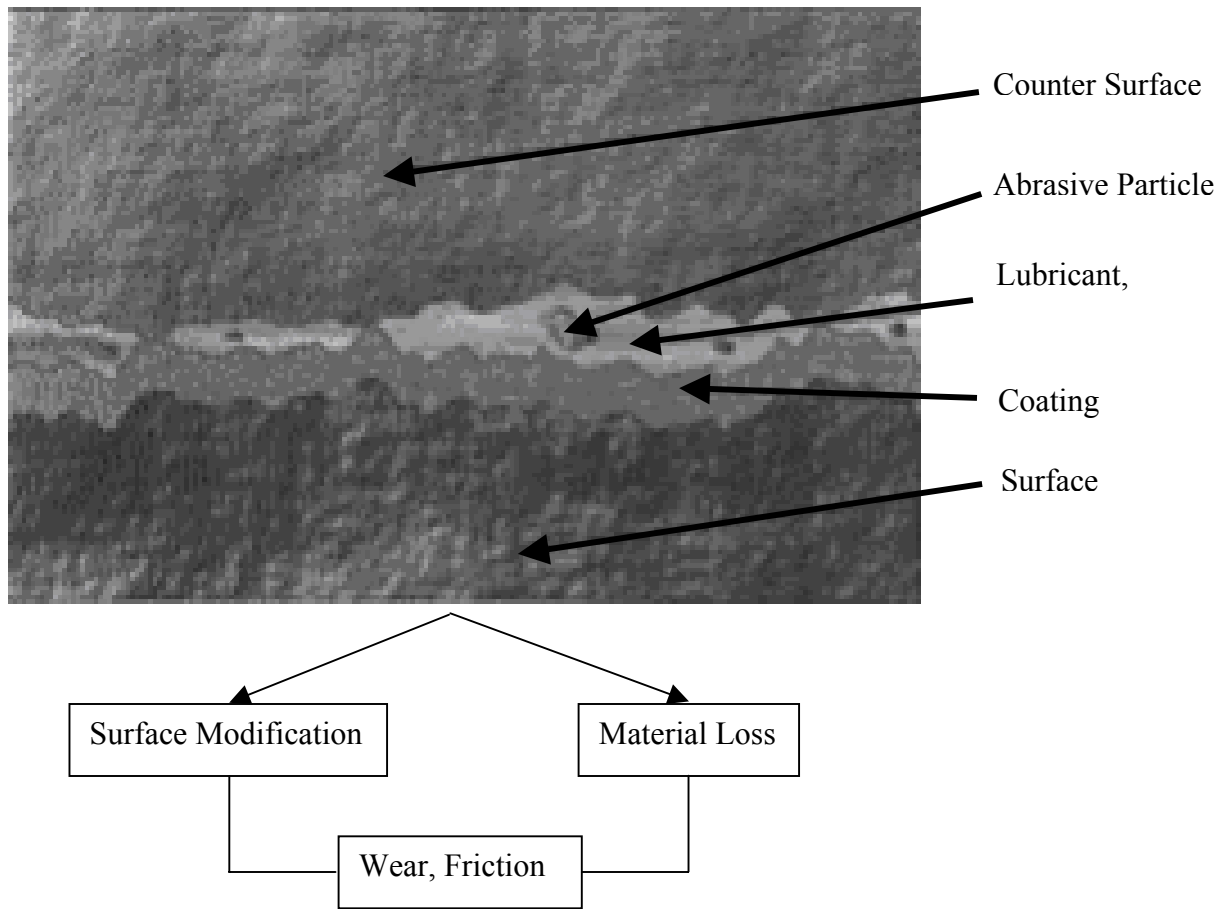


Figure 1: Tribology System

the hard body. During subsequent surface motion cycles, these particles may eventually be removed by fatigue fracture. In more severe cases of adhesive wear, smearing, galling and seizure may occur.

The amount of wear which occurs when two surfaces slide over each other tends to increase with sliding distance and with the normal load acting between the surfaces. Many quantitative models for sliding wear have been developed, but one of the simplest is that due to Archard. It is particularly valuable as a means of comparing wear rates and material behavior under different conditions. The Archard model for sliding wear suggests that wear is associated with interactions between plastically deforming asperities (high spots) on the sliding surfaces, and leads to the simple equation:

$$Q = (K * W) / H$$

where Q is the volume of material removed from the surface by wear per unit sliding distance, W is the normal load applied between the surfaces, and H is the indentation hardness of the softer surface. Many sliding systems do show a relatively linear dependence of wear on sliding distance, and under some conditions also show wear rates which are roughly proportional to normal load. The constant K , usually termed the Archard wear coefficient, is dimensionless and always less than unity. The value of K is of fundamental importance, and provides a valuable means of comparing the severity of different wear processes. The quantity K/H , given the symbol k and sometimes termed specific wear rate, is also useful. The units of k are usually $\text{mm}^3 \text{m}^{-1} \text{N}^{-1}$, representing the volume lost (mm^3) per unit sliding distance (m) per unit normal load on the contact (N). These units are commonly used in quoting experimentally measured rates of wear.

Although in many cases of sliding wear, K is effectively constant over quite large ranges of load or sliding speed, in some instances sharp transitions can occur, and K may change by a factor of 100 or even 1000 for a relatively small change in the conditions. This behavior is associated with a change in the predominant mechanism of material removal; for this reason it is always dangerous to infer the likely rate of wear in a system from data obtained under rather different conditions.

The terms “mild” and “severe” are often used, as for metals, to describe different regimes of wear. Transitions between these regimes lead to sharp changes in wear rate with load, sliding speed, or environmental conditions (e.g., with humidity or atmospheric oxygen content). Mild wear in ceramics is associated with a low wear rate, smooth surfaces and a relatively constant friction force. The mechanisms of wear are dominated by plastic flow (involving low strains in these materials) or tribochemical reactions. The wear debris is often finely divided, and may be chemically different from the bulk material, e.g., through oxidation or hydration. Severe wear, in contrast, causes a higher wear rate together with a rougher surface, a fluctuating friction force, and mechanisms of wear dominated by brittle fracture. The wear debris is often angular, coarse, and not chemically different from the sliding surface.

Severe wear in metals is often described as scuffing, scoring, or galling. Scuffing usually refers to localized surface damage associated with local solid-state welding between the sliding surfaces, and is often used to describe the breakdown of lubrication, at high sliding speeds. The term scoring is sometimes used as a synonym for scuffing as described above, and both terms can also imply scratching by abrasive particles. Galling represents a more severe form of scuffing, due to local welding, and is associated with gross surface damage. The word often refers to damage

caused by unlubricated sliding at slow speeds, characterized by severely roughened surfaces and transfer or displacement of large fragments of material.

Abrasive Wear

Abrasive wear involves the presence of small hard particles between the sliding surfaces. It is a form of cutting wear where the material is removed by hard wear particles, by hard asperities, or by hard particles entering the interface from the environment. The hardness of these particles influences the rate of wear: particles with lower hardness than that of surface cause much less wear than harder particles. The condition of abrasive wear are sometimes classified as “low stress” in which the abrasive particles themselves are relatively undamaged in the wear process, or “high stress” when the particles experience extensive fracture.

Fatigue Wear

Fatigue wear occurs in situations where there is repeated loading and unloading of surfaces in contact. Failure may initiate at both surface flaws or cracks or at subsurface inhomogeneities. Crack growth eventually results in detached wear particles.

Fretting Wear

Fretting wear is a type of fatigue wear that occurs under conditions of oscillatory movement of small amplitude but relatively higher frequencies. Other subsequent damage processes occur

during fretting, including breakup of protective films, adhesion and transfer of material, oxidation of metal wear particles and nucleation of surface cracks.

Delamination Wear

Delamination wear is a form of regular detachments of thin platelike particles from wearing surfaces due to the influence of high tangential (friction) forces in the surface contact zone. During cyclic loading the cracks that develop propagate parallel to surface at a depth governed by the material properties and coefficient of friction.

Oxidation Wear

Oxidation wear arises from the continuous rubbing and removal of surface films produced by reaction with the environment. Wear damage is modest in this case as the oxide grows soon after it is lost. However at high temperatures where chemical reactions are accelerated oxidation wear is aggravated.

Transfer Films

The friction of a tribological system and thereby its wear depends on the existence or the generation of a low shear stress surface or film between the moving counter-surfaces. This low shear stress film

- can be caused at one or both surfaces themselves (e.g., sulfide coatings);
- can be introduced from outside of the system (lubrication); or

- can be generated by the rubbing surfaces themselves (e.g., DLC coatings).
- In the case of very smooth hard surfaces with extremely low chemical potential also the interface itself might play the role of the low shear stress surface.

Application-oriented Optimization of Tribological Coatings

The ideal tribological film would be one sustaining extremely high normal pressures and adhering very well to the substrate. The ideal tribological film would also be extremely hard and tough, i.e., show no wear at all and it would be extremely stable even at high temperatures occurring, for example, in dry machining operations. In reality no coating can fulfill all these requirements. So for each service condition a compromise has to be found and it also has to be taken into account that the substrate material plays an important role in determining the lifetime of the whole system.

In general the following requirements should be fulfilled for a long lifetime of the coating substrate system:

- A substrate being hard and tough enough to carry the load in the temperature range of service.
- A roughness being low enough such that the coating does not fail by rubbing away of the roughness peaks.
- A coating that decreases shear stresses by lowering the friction.
- A coating having a high wear resistance in the particular tribological situation.

To fulfill these functional demands, an adequate adhesion between coating and substrate as well as an adequate load carrying capacity are both essential. Also for effective design of tribological coatings, both substrate properties such as hardness, surface roughness, corrosion

resistance, material homogeneity, etc and coating properties such as thickness, adhesion, mechanical properties, internal stress, etc need to be optimized.

The most commonly employed techniques for deposition of tribological coatings are PVD and CVD by DC and RF magnetron sputtering. An important benefit of PVD and CVD processes is the high flexibility as to composition and structure of the coatings [12]. The most common PVD and CVD coating materials are nitrides (TiN, CrN, BN etc.), carbides (TiC, CrC, W₂C, WC/C, etc.), oxides (e.g. alumina) or combinations of these. In addition to these material groups, MoS₂, DLC and diamond have also been used successfully. Amorphous DLC forms a large group of coatings. They can be doped with metals, nitrides and carbides to further improve the mechanical and tribological properties and to enhance the adhesion to the substrate. Under suitable conditions, DLC can provide a combination of good wear and corrosion resistance and a low friction [12]. DLC can be deposited by microwave chemical vapor deposition process (MWCVD). [16]

The coatings that are being studied elsewhere for tribological application are titanium nitride [17-21], titanium carbide (TiC) [21], titanium carbonitride Ti (C, N) [22], chromium nitride (CrN) [23-24], chromium carbide (CrC) and their combination, as well as diamond like carbon and diamond coatings [21, 25-31].

Application of Tribological Coatings to the Two Stage Reverse Turbo Brayton Cycle (RTBC)

CryoCooler

Hydrogen is a clean and sustainable form of carrier of energy that can be used in mobile and stationary applications. Hydrogen can be stored as liquid hydrogen, compressed hydrogen and bonded hydrogen as metal/liquid hydrides or adsorbed carbon compounds. Near term spaceport

operations are one of the prominent applications for usage of large quantities of liquid hydrogen as a cryogenic propellant. Efficient storage and transfer of liquid hydrogen is essential for reducing the launch costs. Near term spaceport operations are one of the prominent applications for usage of large quantities of liquid hydrogen as a cryogenic propellant. All the previous attempts of cryocoolers by NASA for zero boil-off (ZBO) of cryogenic propellants in space have cooling powers of less than 2 W at liquid hydrogen temperature. These versions of flight-like cryocoolers would be more appropriate for cooling of sensors and super conducting materials in a spacecraft but would prove unsuitable for ZBO applications. The present cryocooler under development with 50 W of cooling power at liquid hydrogen temperature would be ideal for ZBO of cryogenic propellants in NASA's future robotic missions to Mars and for other human space missions. One part in development of the cryocooler is to reduce the friction and wear between mating parts thus increasing its efficiency. Tribological coatings having extremely high hardness, ultra-low coefficient of friction, and high durability at temperatures lower than 60 K are being developed to reduce friction and wear between the mating parts of the cryocooler thus improving its efficiency.

The use of microfabrication technologies in the miniaturization of the cryocooler enables higher reliability and allows relatively high thermodynamic efficiencies of the turbine and the compressor in a small footprint. However, despite great progress made through the past half century, many basic issues in fundamental tribology such as origin of friction and failure of lubrication have remained unsolved. Better understanding of the intimate mechanisms of friction, lubrication, and other interfacial phenomena at the atomic and molecular scales is expected to provide designers and engineers the required tools and capabilities to control and monitor friction, reduce unnecessary wear, and predict mechanical faults and failure of lubrication in microelectronic mechanical systems and nano-devices. Moreover, as mentioned earlier a

tribological system is application dependent and is composed of elements such as the structure (contact materials, and contact geometry), the operating conditions (loads, stresses, duration of operation), and the environment and surface conditions (surface topography, ambient temperature).

Nitrides of high-melting-point metals (e.g. TiN, ZrN) and diamond-like-carbon are potential candidates for cryogenic applications as these coatings have shown good friction behavior and wear resistance at cryogenic temperatures. These coatings are known to have coefficient of friction less than 0.1 at room temperature. However, cryogenic environment leads to increase in the coefficient of friction. It is expected that a composite consisting of a base layer of a hard coating covered with layer having an ultra-low coefficient of friction would provide better performance. Extremely hard and extremely low friction coatings of titanium nitride, molybdenum disulphide, TiN/MoS₂ bilayer coatings, DLC and DLC/MoS₂ bilayer coatings have been chosen for this application. TiN film was deposited by reactive DC magnetron sputtering system from a titanium target and MoS₂ film was deposited by RF magnetron sputtering using a MoS₂ target. Microwave assisted chemical vapor deposition technique was used for preparation of DLC coatings. These composite coatings contain a solid lubricating phase and a hard ceramic matrix phase as distinctly segregated phases. These are envisioned as having the desired combination of lubricity and structural integrity [32]. Extremely hard coatings of TiN and DLC were chosen to provide good wear resistance and MoS₂ was chosen as the lubricating phase as it provides excellent solid lubricating properties due to its lamellar crystal structure.

This thesis presents preparation; characterization (SEM and XRD), microhardness and tribological measurements carried out on TiN and TiN/MoS₂ coatings on aluminum and glass substrate at room temperature. It also presents initial development in preparation of DLC coatings.

EXPERIMENTAL TECHNIQUES

A 15.24 cm six-way cross vacuum chamber pumped with a turbomolecular pump-mechanical pump combination and fitted with two 7.62 cm diameter magnetron sputtering sources bonded with a water-cooled backing plate were used for deposition of the TiN and MoS₂ films on glass and aluminum substrates with no substrate biasing. The substrates were fixed to a holder at a distance of 5 cm facing the target. The chamber was pumped to a base pressure of 10⁻⁶ Torr. Prior to the film deposition, the target was sputter cleaned for 5 min with an Ar pressure of 20 mTorr. The TiN film was deposited by reactive DC magnetron sputtering system from a titanium target (7.62 cm diameter and 0.64 cm thickness). Number of depositions of TiN films were carried out by varying the total pressure and also the proportion of argon to nitrogen. The series of TiN films with different deposition parameters are described in detail in this chapter. Characteristic golden color of TiN films was achieved. The limit in terms of varying the argon to nitrogen ratio was reached as the films indicated greater porosity and signs of peeling off. The sputtering parameters for deposition of TiN layer were thus optimized so as to minimize the residual stresses developed during deposition. Therefore, the TiN film deposited is a multilayered film with a first layer of only pure Ti with Ar pressure maintained to assure a good bonding between the coating and substrate. The second layer is a TiN film is deposited at a higher total pressure of Ar and N₂. The third layer is also a TiN film deposited at a total lower pressure by reducing the Ar content of the mixture and maintaining the nitrogen content to be same. These layered structures reduce the residual stress developed in the film and film thickness in the range of 1 μm were deposited with a total deposition time of about 30 min. Dektak Profilometry showed good thickness uniformity of TiN films. MoS₂ film was deposited by RF magnetron sputtering using a MoS₂ target (7.62 cm

diameter and 0.64 cm thickness). The film parameters were optimized and depositions were carried out with Argon pressure maintained at 10 mTorr and forward power of 100 watt. The deposition time was 20 min resulting in film thickness in the range of 0.5-0.6 μm . Dektak Profilometry showed good thickness uniformity of MoS_2 films. The bilayer coating of TiN/ MoS_2 was deposited using the above-optimized parameters for both the films. The microstructure of the film is determined by the deposition parameters.

Formation of crystallographic phase was studied using X-ray diffraction (XRD) in a Rigaku X-ray diffractometer. Surface morphology and chemical composition were studied by scanning electron microscopy (SEM) using high resolution JEOL 6400 scanning electron microscope attached with energy dispersive analysis of X-rays (EDAX) at MCF. Film thickness was measured on DEKTAK profilometer.

Substrate Preparation

Various sizes of glass, aluminum and Si-wafer substrates were used for deposition of TiN and MoS_2 film and were cleaned using the procedure described below. An aluminum tray was made to hold the substrate for ultrasonic cleaning. The cut substrate was kept in this tray. It was immersed in a 50/50 solution of soap and water and was subjected to ultrasonic cleaning for 15 minutes. The substrate was removed and thoroughly cleaned with flowing tap water to remove any traces of soap. It was then rinsed in distilled deionised water. The tray was cleaned and substrate was transferred back to it. Isopropanol was poured in the tray and the substrate was again subjected to ultrasonic cleaning for 10 minutes. The substrate was then rinsed thoroughly in deionised water and was finally blow-dried using jet of compressed nitrogen gas.

Sputtering Chamber for Deposition - TiN and MoS₂ film

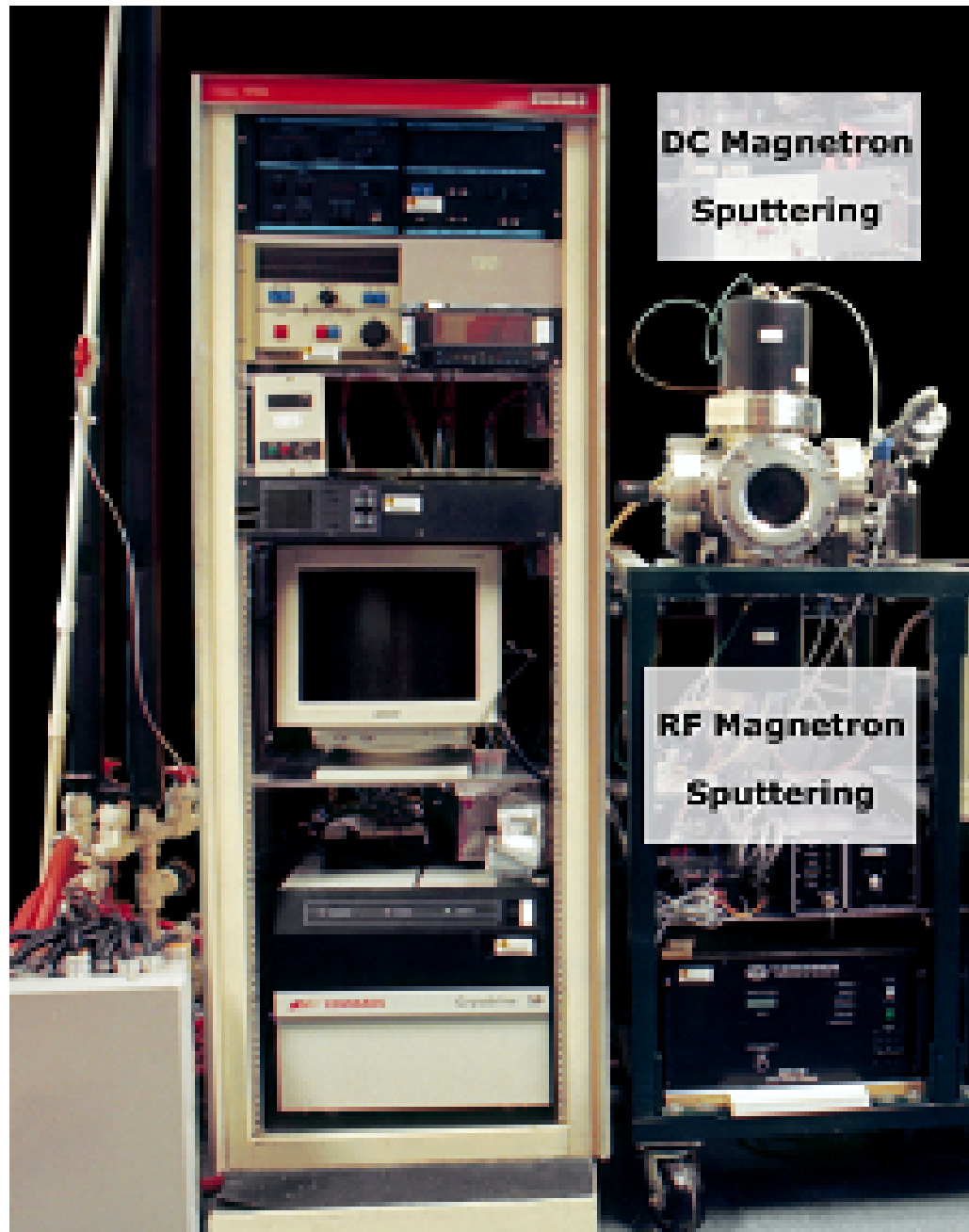


Figure 2: Sputtering Chamber

The sputtering system as shown in Figure 2 consists of a 15.24 cm six-way cross vacuum chamber pumped with a turbomolecular pump-mechanical pump combination and fitted with two 7.62 cm diameter magnetron sputtering sources bonded with a water-cooled backing plate were used for deposition of the TiN and MoS₂ films on glass and aluminum substrates with no substrate biasing. The six-way cross vacuum chamber was initially thoroughly cleaned with soap, water and alcohol to remove any contaminants from any previous depositions of other materials and was dried thoroughly. Any vacuum leaks were removed by conducting leak tests by using a Residual Gas Analyzer (RGA) and leaks were eliminated so as to improve the vacuum to lower orders of 10⁻⁶ Torr.

Series of Deposition of TiN Layer

Number of deposition on glass and aluminum substrates with different deposition parameters were carried out by varying the total pressure and also the proportion of argon to nitrogen. The limit in terms of varying the argon to nitrogen ratio was reached as the films indicated greater porosity and signs of peeling off. The sputtering parameters for deposition of TiN layer were thus optimized so as to minimize the residual stresses developed during deposition.

Series-1 - TiN Film

The initial series-1 of depositions were carried out by RF reactive magnetron sputtering on glass substrate by using forward power in the range 80-150 watt and adjusting the proportion of nitrogen to argon sputtering gas. The reflected power obtained during the depositions were high and therefore, the RF cable from the RF tuner to the target was shortened to obtain an impedance

matching at the RF frequency of 13.56 MHz and consequently to minimize the reflected power. The deposition parameters are listed in Table 3. DC magnetron sputtering was used to achieve film thickness of over 1 micron.

Series-2 - TiN Film

Thickness obtained during the Series-1 depositions was under 1 micron and therefore DC magnetron sputtering was used. Additional TiN samples on glass and aluminum substrates were prepared by DC reactive magnetron sputtering. The deposition parameters are listed in Table 4.

Series-3 - TiN Film

The hardness achieved for the series-2 TiN films were not high and was expected to show inferior tribological properties. Therefore, additional TiN samples on glass and aluminum substrates were prepared by DC reactive magnetron sputtering. The deposition parameters are listed in Table 4.

Deposition of MoS₂ Film

RF magnetron sputtering was used to deposit MoS₂ film with a MoS₂ target (7.62 cm diameter and 0.64 cm thickness). Number of deposition on glass and aluminum substrates with different deposition parameters was carried out by varying the Argon pressure and power. The film parameters were optimized and depositions were carried out with Argon pressure maintained at 10 mTorr and forward power of 100 watt. The deposition time period of 15-20 min resulted in film

thickness in the range of 0.5-0.6 μm . Dektak Profilometry showed good thickness uniformity of MoS_2 films.

Table 3: Deposition parameters of Series-1 TiN samples

Series # - Sample #	Deposition Time (hour)	Nitrogen Pressure (mtorr)	Argon Pressure (mtorr)	Forward Power (watt)	Avg. Coating Thickness (Angstrom)	Remarks	
Sr1-Sp 1	4	1	4	80	5700	Grayish Film	RF
Sr1-Sp 2	4	1	5	100	7500	Grayish Film	RF
Sr1-Sp 3	4	0.5	5	100	6600	Grayish Film	RF
Sr1-Sp 4	4	0.5	5	120	6100	Grayish Film	RF
Sr1-Sp 5	4	1.5	5	100	6400	Grayish Film	RF
Sr1-Sp 6	4	1.5	5	120	2500	Grayish Film	RF
Sr1-Sp 7	5	0.5	5	150	3600	Grayish Film	RF
Sr1-Sp 8	5	0.5	5	120	1150	Grayish Film	RF
Sr1-Sp 9	5	0.5	5	150	1600	Grayish Film	RF

Table 4: Deposition parameters of Series-2 TiN samples

Series # - Sample #	Deposition Time (hour)	Nitrogen Pressure (mtorr)	Argon Pressure (mtorr)	Forward Power (watt)	Avg. Coating Thickness (Angstrom)	Remarks	
Sr2-Sp 1	2	0.5	6	150	14379	Grayish Film	DC
Sr2-Sp 2	1.5	0.5	4	150	8096	Grayish Film	DC
Sr2-Sp 3	2	0.5	4	150	10120	Grayish Film	DC
Sr2-Sp 4	2	1	4	150	11575	Grayish Film	DC
Sr2-Sp 5	2	1.5	4	150	10866	Grayish Film	DC
Sr2-Sp 6	2	0.5	6	150	16206	Grayish Film	DC
Sr2-Sp 7	2	0.5	4	150	10737	Grayish Film	DC
Sr2-Sp 8	2	1	4	150	13368	Grayish Film	DC
Sr2-Sp 9	2	1.5	4	150	12007	Grayish Film	DC

Table 5: Deposition parameters of Series-3 TiN samples

Series # - Sample #	Deposition Time (hour-min)	Nitrogen Pressure (mtorr)	Argon Pressure (mtorr)	Forward Power (watt)	Avg. Coating Thickness (Angstrom)	Remarks	
Sr3-Sp 1	Total Dep. Time: 1 hr 40 min			150	No step to measure thickness on Al substrate	Golden Film	Al Substrate
	30 min	1.5	5				
	30 min	1.5	1.5				
	10 min	1.5	5				
	30 min	1.5	1.5				
Sr3-Sp 2	Total Dep. Time: 1 hr 40 min			150	No step to measure thickness on Al substrate	Golden Film	Al Substrate
	30 min	0.5	2.5				
	30 min	0.5	0.5				
	10 min	0.5	2.5				
	30 min	0.5	0.5				
Sr3-Sp 3	Total Dep. Time: 55 min			150	12000-125000	Golden Non- porous	Glass Substrate
	15 min	-	5.5				
	15 min	1	5				
	25 min	1	1				
Sr3-Sp 4	Total Dep. Time: 55 min			150	No step to measure thickness on Al substrate	Golden	Al Substrate
	15	-	5.5				
	15	1	5.5				
	25	1	1				

Deposition of TiN/MoS₂ Film

The optimized parameters obtained for TiN and MoS₂ film were used to deposit bilayer coating of TiN and MoS₂ film on glass and aluminum. These optimized parameters were further adjusted slightly in terms of time to control the thickness obtained during deposition and to prevent peeling of films due to stress developed due to higher film thickness.

The coefficient of friction and wear measurements on TiN/MoS₂ bilayer coating on Si wafer were planned to be carried out on the “Tytron™ 250 MicroForce Testing Equipment” with the assistance of Dr. Quanfang Chen and his colleagues at UCF. These measurements require the film to be deposited on three 0.9 mm diameter bumps on 1 cm x 1 cm silicon wafer to minimize the contact area between two rubbing samples as shown in Figure 3 and providing more accurate coefficient of friction and wear measurements. The silicon sample preparation involved the design and fabrication of the mask (Figure 4) required to obtain these bumps on the wafer. The wet and dry oxidation of the silicon wafer was carried out to grow a 3-micron layer of silicon dioxide. Photolithography method was used to carry out the masking and etching of the wafer to define these bumps on the wafer. TiN/MoS₂ films were deposited using the optimized parameters on 1 cm x 1 cm silicon wafers with and without these bumps for the friction and wear measurements. The deposition parameters are provided in Table 6.

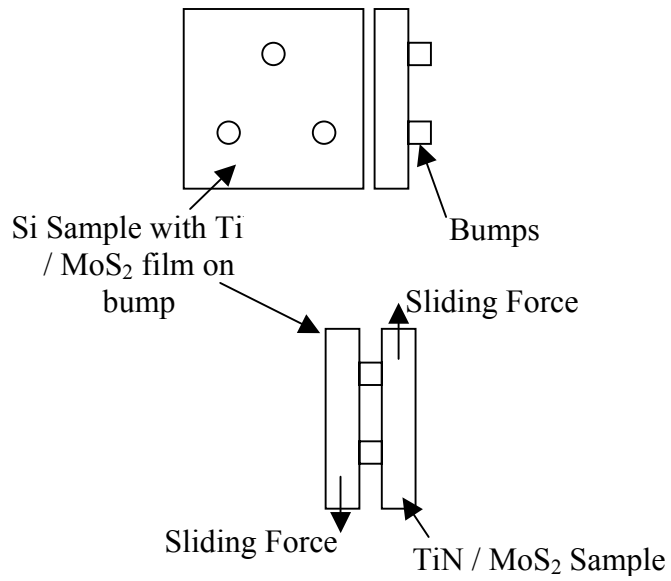


Figure 3: Bumps on Si-wafer and sliding action

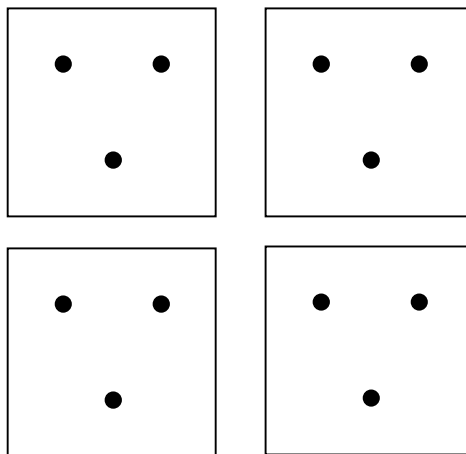


Figure 4: Mask Design

Table 6: Deposition parameters of TiN/MoS₂ samples

Series # - Sample #	Deposition Time (hour-min)	Nitrogen Pressure (mtorr)	Argon Pressure (mtorr)	Forward Power (watt)	Avg. Coating Thickness (Angstrom)	Remarks	
Samp-1	Total Dep. Time: 30 min - TiN			150	No step to measure thickness on Al substrate	Golden Non-porous Film	Al Substrate
	7 min	-	5.5				
	8 min	1.0	5.5				
	15 min	1.0	1.0				
	Total Dep. Time: 15 min – MoS₂						
	15 min	-	10	100	Blackish		
Samp-2	Total Dep. Time: 30 min - TiN			150	10500-11500	Golden Non-porous Film	Glass Substrate
	7 min	-	5.5				
	8 min	1.0	5.5				
	15 min	1.0	1.0				
	Total Dep. Time: 15 min – MoS₂						
	15 min	-	10	100	Blackish		
Samp-3	Total Dep. Time: 30 min - TiN			150	13000-13500	Golden Non- porous	Glass Substrate
	7 min	-	5.5				
	8 min	1.0	5.5				
	15 min	1.0	1.0				
	Total Dep. Time: 25 min – MoS₂						
	15 min	-	15	65	Blackish		
	10 min	-	10	100			
Samp-4	Total Dep. Time: 30 min - TiN			150	14500-15000	Golden	Glass Substrate
	7 min	-	5.0				
	8 min	1.0	5.0				
	15 min	1.0	1.0				
	Total Dep. Time: 28 min – MoS₂						
	15 min	-	15	65	Blackish		
	13 min	-	10	100			

RESULTS AND DISCUSSION

Series-1 TiN Film Results and Discussion

The initial series-1 of depositions were carried out by RF reactive magnetron sputtering on glass substrate by using forward power in the range 80-150 watt and adjusting the proportion of nitrogen to argon sputtering gas. These films were grayish in color and did not have a characteristic golden color of TiN films. They had thickness in the range of 1600 – 7500 angstroms depending on the deposition parameters: ratio of argon to nitrogen content, total pressure, deposition time and power. As these coatings were less than a micron thick and were not of the characteristic golden nature of TiN film no further characterization was carried out. DC magnetron sputtering was used to achieve film thickness of over 1 micron in the subsequent experiments.

Series-2 TiN Film Results and Discussion

Initial depositions of titanium nitride (hard coating) on glass and aluminum substrate were carried out using DC reactive magnetron sputtering by using forward power in the range 80-150 watt and adjusting the proportion of nitrogen to argon sputtering gas.

EDS analysis (Table 7) showed that films have good stoichiometric ratio of Ti and N, and therefore, it was inferred that fully reacted TiN coatings have been obtained. Peel test showed good adhesion of TiN coatings with glass substrates. Dektak Profilometry showed good thickness uniformity of TiN films. Results of microhardness measurement carried out with the assistance of Dr. Raj Vaidyanathan and his colleagues at UCF for the above samples are shown in Table 7.

Table 7: Series 2 - EDS analysis and results of microhardness measurement.

Series # - Sample #	N ₂ : Ar Ratio	Atomic Percent Nitrogen: Titanium	Average Hardness		Average Elastic Modulus (GPa)
			GPa	HV (Kgf/mm ²)	
Sr2-Sp 1	0.5: 6	N :Ti = 50.3:49.7	9.32	878.47	144.20
Sr2-Sp 2	0.5 : 4	N:Ti = 53.05:46.95	-----	-----	-----
Sr2-Sp 4	1: 4	N:Ti = 52:48	16.62	1567.02	200.21

HV –Vicker’s Hardness

Structural Characterization by XRD

There are three different titanium nitrides; a tetragonal nitride, Ti₂N, the body centered tetragonal (bct) titanium nitride, δ', and the face-centered cubic (fcc) tetragonal nitride, TiN. This last nitride exists over a large nitride range, from 28 to >50 atom% N, and has a NaCl prototype [32]. The type of bonding in the fcc nitride is characterized by partly covalent and partly metallic [33] and the exact nature is largely influenced by the exact chemical composition. Even though titanium nitride is stable over a broad composition range, its structure and properties depend critically on the actual composition [34]. The NaCl structure of the TiN phase has at the stoichiometric composition lattice parameter of 4.240 Å. Because of the vacancy defect structure that is stable over a broad composition range the lattice parameter decreases for both overstoichiometric and understoichiometric films [34]. These deviations are caused by different phenomena such as

- differences in thermal expansion coefficient between the films and the substrates causes stresses in the films that are reflected in the lattice parameter.

- high compressive stresses due to argon incorporation are often obtained for sputtered films , thus expecting changes in the lattice parameter.
- Incorporation of nitrogen interstitially in the lattice in tetrahedral positions results in expansion of lattice.

For pure films around the stoichiometric composition, the most probable cause is intrinsic stresses generated by, for example, a small grain size, a high defect density or the incorporation of argon or nitrogen interstitially in the lattice [34].

XRD analysis for thin film samples was carried out at CREOL with values of 2θ in the range from 30° to 80° and step size of 0.02° . The strongest reflection was from (111) at 2θ value of 37.04 radian. XRD patterns provided in Figure 5 show that the initial TiN films developed preferred {111} orientation. This plane is the closest packed surface with the lowest surface energy. Close packed plane are also slow growth planes and such planes are know to survive at the expense of fast growth planes. The peak for sample Sr2-Sp4 is sharper compared to that for sample Sr2-Sp1 in figure 5, indicating a more crystalline nature and a higher degree of {111} preferred orientation. Consequently the sample Sr2-Sp4 is expected to have higher hardness. In fact, this is confirmed by the hardness measurements provided in Table 7 for the two samples.

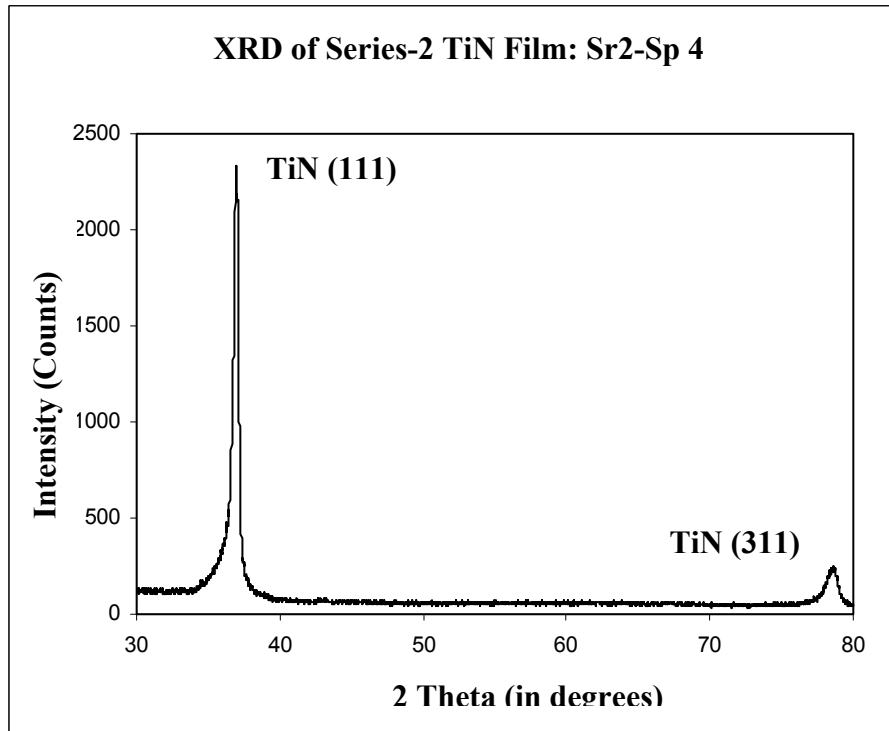
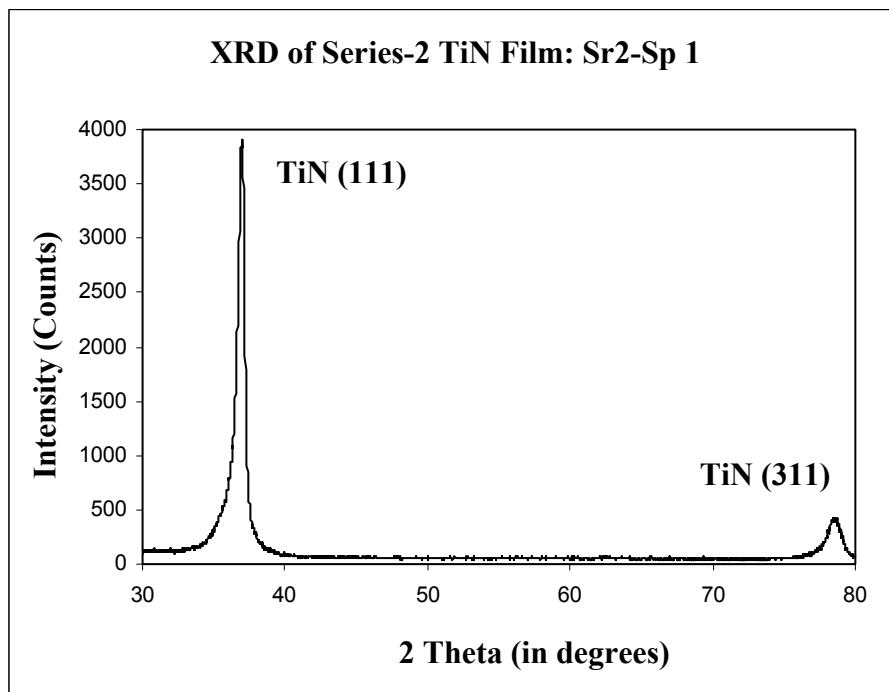


Figure 5: XRD Patterns of Series-2 - TiN (Sr2-Sp 1 and Sr2-Sp 4) with (111) peak orientation.

Series-3 TiN Film Results and Discussion

The hardness obtained during the Series-2 films was not high as compared to literature values. Multilayered films were grown in this series as they provide improved film density, lubrication and hardness [35]. Also multilayered coatings consisting of ceramic and metallic material have higher fracture toughness [35]. TiN layers were grown with the first layer at higher pressure to develop large grains to improve the adhesion of film to the surface and the consecutive second TiN layer was grown at lower pressure to facilitate small grains sizes and therefore resulting in more hardness. Initially the films were consisting of 4-6 layers alternate layers of TiN at high and low total pressures. However, the release of internal stress in the film cause breaking of the film. The layers were then reduced to only two TiN layers which provided adequate thicknesses as well as did not peel off due to internal stress developed in the film. A Ti underlayer was also deposited before the deposition of TiN layers to increase the adhesion of film and to facilitate increase in thicknesses.

The sputtering parameters for deposition of TiN layer were thus optimized so as to minimize the residual stresses developed during deposition. Therefore, the TiN film deposited is a multilayered film with a first layer of only Ti with Ar pressure maintained at 5 mTorr. This pure Ti layer is grown to assure a good bonding between the coating and substrate. The second layer of TiN is deposited at a forward power of 150 watt with the Ar pressure maintained at 5 mTorr and N₂ pressure maintained at 1 mTorr. The third layer of TiN is also deposited at a forward power of 150 watt with Ar pressure maintained at 1 mTorr and N₂ pressure maintained at 1 mTorr. These layer structures reduce the residual stress developed in the film and film thickness in the range of 1 μ m were deposited with a total deposition time of approximately 30 min. The lower pressure during the deposition of the final layer at provides higher ionization of sputtering gas and an

increased rate of ion bombardment during the growth. This can result in increased hardness mainly because of the compressive residual stress developed in the film. Voids in grain boundaries give rise to low hardness [34].

Peel test showed good adhesion of TiN coatings with glass substrates. Dektak Profilometry also showed good thickness uniformity of TiN films. Energy dispersive analysis of X-rays showed that TiN film (Sr3-Sp3) had near equal stoichiometric ratio of Ti and N (Atomic Percent N : Ti = 52.91:47.09).

Surface Morphology and Structural Characterization by XRD

Surface morphology study of TiN film (Sr3-Sp3) on glass substrate was performed at the Material Characterization Facility (MCF) using scanning electron microscope. A scanning electron microscopy image of TiN film (Sr3-Sp3) is shown in Figure 6. The grains appear to be nanocrystalline in nature. The surface of the TiN specimen appears to be smooth, flat and dense with fine grain structure and displays characteristic golden color. The broad nature of peaks in X-ray diffraction pattern (Figure 7) confirmed the nanocrystalline nature of the TiN film (Sr3-Sp3). Prominent peaks of face-centered cubic phase were observed at 111, 200, and 311. The strongest reflection was from (111) at 2θ value of 36.22 radian.

Microhardness Measurements by MTS Tester

Microhardness measurement was carried out at University of South Florida with the help of Dr. Kumar and his colleagues. The loading and unloading curve for the TiN sample (Sr3-Sp3) is provided in Figure 8 and the hardness and modulus values are provided in Table 8.

Microhardness measurements of TiN coating (Sr3-Sp3) on a glass substrate by MTS tester using a Berkovich diamond tip gave average hardness value of 24.90 GPa and average elastic modulus value of 256.60 GPa.

TEM Micrographs

The TEM micrographs of the TiN sample (Sr3-Sp3) are provided in Figures 9-11. Figure 9 shows the TEM cross-section of the TiN sample (Sr3-Sp3). The glass substrate, pure Ti layer, TiN layer and the platinum layer are all clearly visible. Focused Ion Beam was used to prepare the TEM sample. Platinum layer is deposited to prevent the surface damage during the sample preparation by the ion bombardment. TiN layer appears to have a dense columnar structure. Figure 10 shows the interface between Ti layer and the glass substrate. The interface between the coating and substrate appears to be good. The slight delamination observed in this figure is not actually observed in the TEM instrument and appears to be some holographic effect captured in the picture. Figure 11 shows the interface between the Ti layer and the TiN layer. It is also very good.

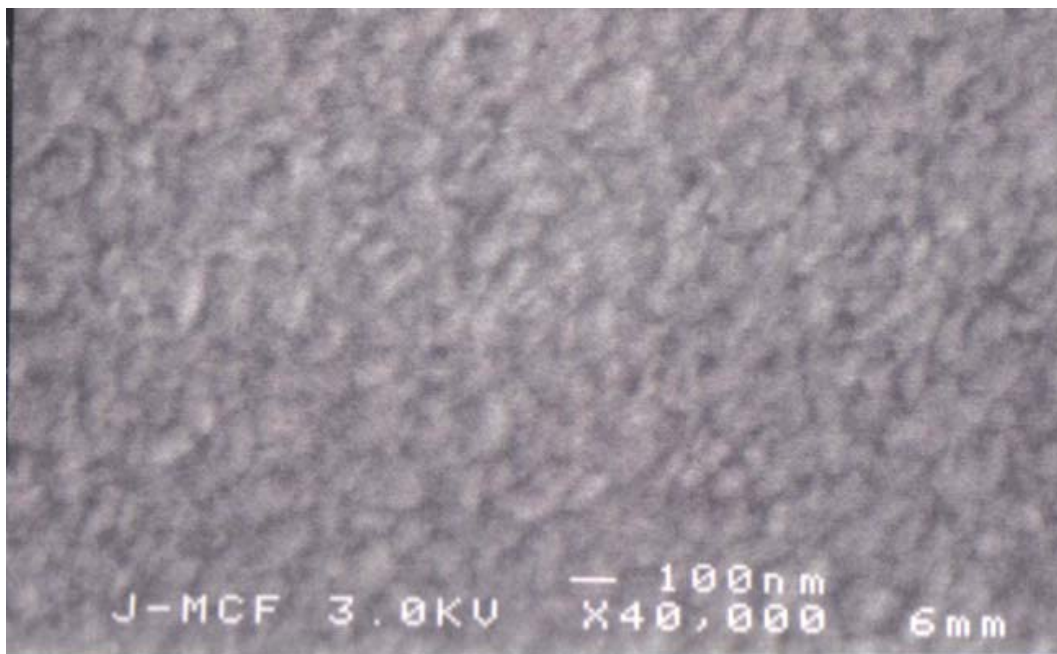


Figure 6: Scanning Electron Microscopy image Series-3 - TiN (Sr3-Sp 3)

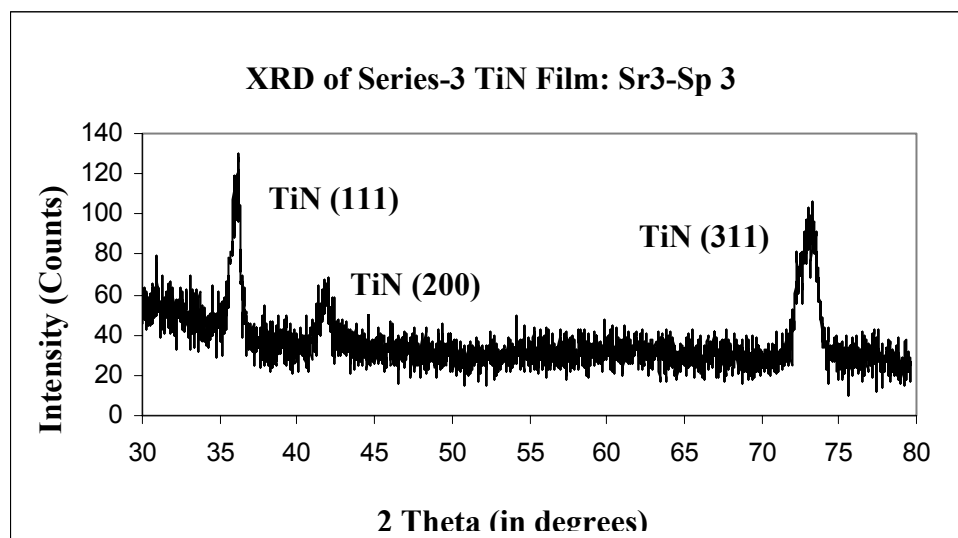


Figure 7: XRD Pattern of Series-3 - TiN (Sr3-Sp 3)

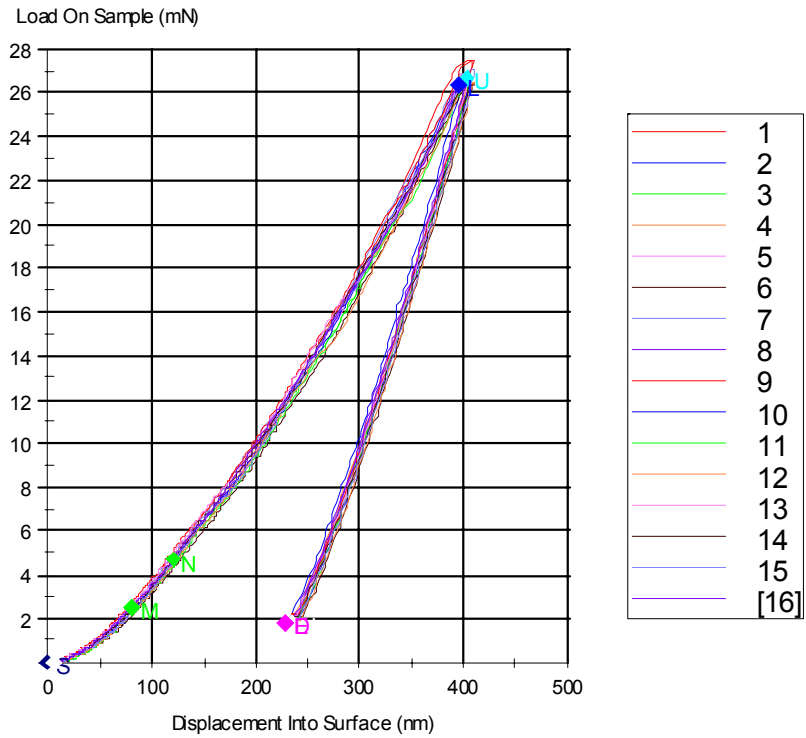


Figure 8: Loading-unloading Curve for TiN samples of Series-3 - TiN (Sr3-Sp 3)

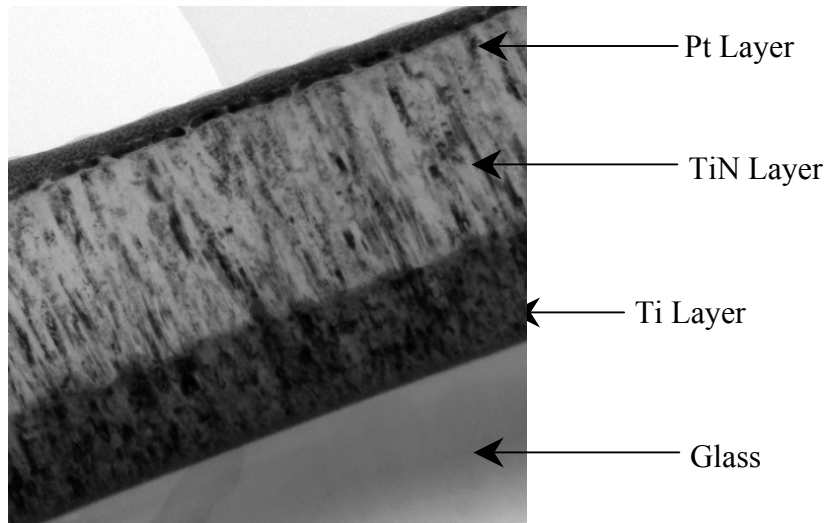


Figure 9: TEM Cross-section showing Glass/Ti/TiN/Pt Layer

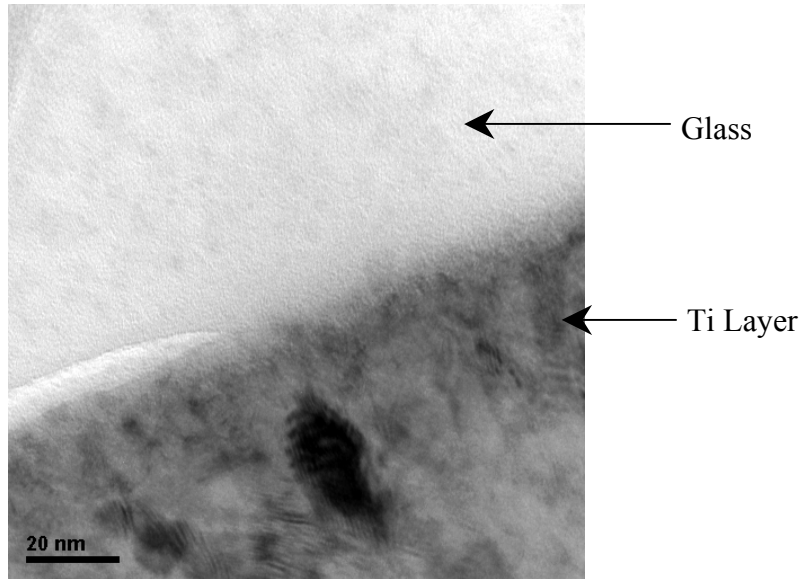


Figure 10: Interface - Glass to Ti Layer at magnification of 130K

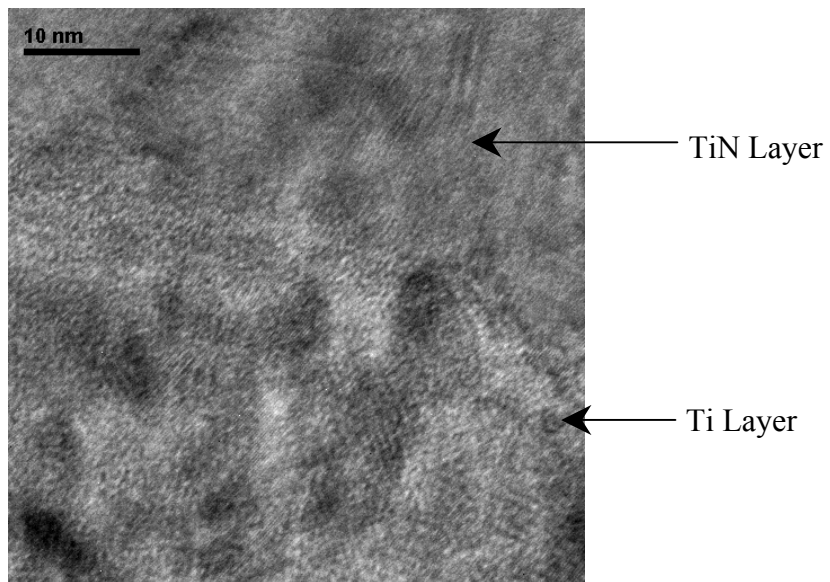


Figure 11: Interface - Ti Layer to TiN layer at magnification of 390K

Table 8: Hardness values for Series-3 TiN sample (Sr3-Sp3)

Test #	E Average Over Defined Range GPa	H Average Over Defined Range GPa	Modulus From Unload GPa	Hardness From Unload GPa	Drift Correction nm/s
1	267.036	25.249	112.103	13.137	0.078
2	246.079	25.030	114.184	12.995	0.071
3	254.806	23.636	110.676	12.699	0.060
4	258.184	26.244	110.332	13.029	0.055
5	249.919	23.500	110.351	12.455	0.053
6	239.967	22.056	107.588	12.416	0.037
7	272.218	26.544	112.155	13.024	0.033
8	255.854	24.653	109.092	12.947	0.041
9	281.735	26.585	109.716	13.116	0.033
10	248.918	25.125	109.844	12.753	0.025
11	245.147	23.619	109.665	12.471	0.042
12	247.110	24.341	105.434	12.787	0.029
13	276.264	27.138	114.001	12.635	0.022
14	253.361	25.475	111.511	12.568	0.027
15	245.411	24.515	109.265	12.557	0.027
16	263.625	24.641	111.191	13.037	0.024
Mean	256.602	24.897	110.444	12.789	0.041
Std. Dev	12.315	1.335	2.192	0.253	0.017

Friction and Wear Tests on Series-3 TiN samples

The coefficient of friction (COF) is not only an intrinsic property of a material and depends on a number of factors such as materials in contact, contact geometry, environment and surface conditions, temperature and method of deposition and the load parameters. The coefficient of friction tests were carried out by ball-on-disc method on TiN sample (Sr3-Sp4) on aluminum substrate with the assistance of Dr. Gregory Sawyer and his colleagues at University of Florida. Friction tests were also carried on TiN sample (Sr3-Sp4) out at University of South Florida with the assistance of Dr. Kumar and his colleagues by pin-on-disc method. The summary of the friction tests is shown in Table 9. The summary of the wear tests is shown in Table 10. Both friction and wear tests were carried out at room temperature. Figure 12 and Figure 13 shows the friction and wear tests on TiN sample (Sr3-Sp4) by pin-on-disc method at University of South Florida. Figure 14 shows TiN coated aluminum substrate and the inside of an aluminum ring. Both friction and wear tests shows that the coating provided low friction and good wear resistance.

Table 9: Summary of friction tests by ball-on-disc and pin-on-disc method on Series-3 TiN films

Series # Samp. #	Trib. Coating	Coating Pair	Subs.	Method	Speed (RPM)	Force (gm)	COF Range	Average COF
Sr-Sp4	TiN	Steel Ball	Al	A	-	100	0.50 - 0.60	0.55
Sr-Sp4	TiN	TiN coated Steel Ball	Al	A	-	50	0.18 - 0.22	0.20
Sr-Sp4	TiN	3/16 diam alumina ball	Al	B	42	66.3	0.14 - 0.16	0.15

A = pin-on-disc method
B = ball-on-disc method

Table 10: Summary of wear tests by pin-on-disc method on Series-3 TiN films

Series # Samp. #	Trib. Coating	Coating Pair	Subs.	Force (gm)	Cycles #	COF Range	Average COF
Sr-Sp4	TiN	Steel Ball	Al	100	300	0.6 - 0.75	0.675
Sr-Sp4	TiN	TiN coated Steel Ball	Al	50	300	0.22 - 0.28	0.25

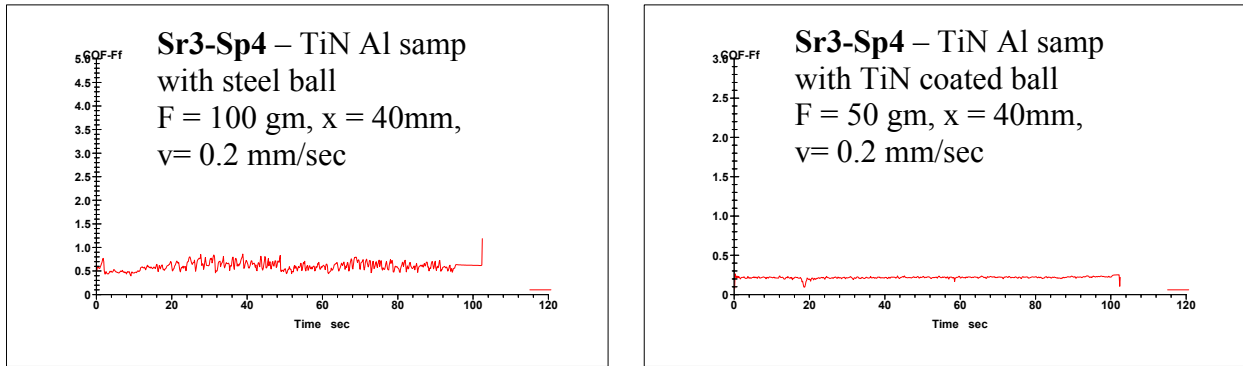


Figure 12: Friction tests of TiN Sample (Sr3-Sp4) with steel ball and TiN coated ball

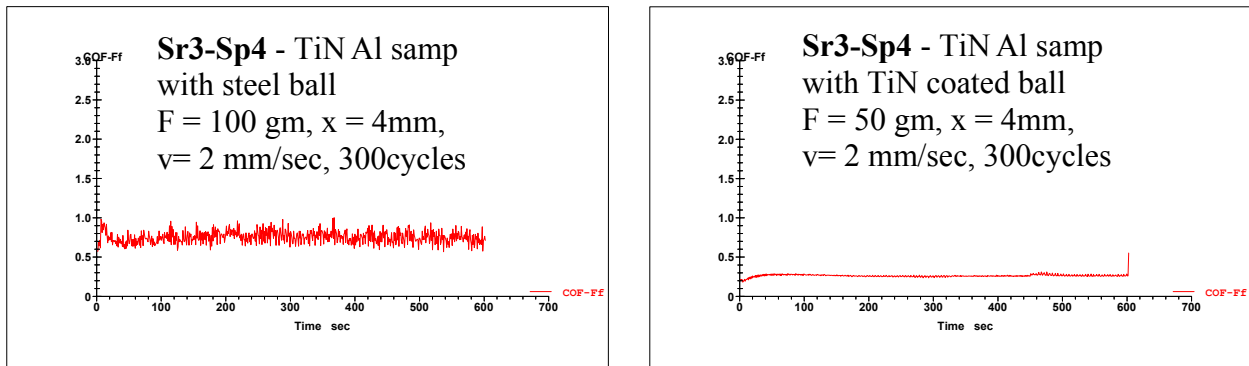


Figure 13: Wear tests of TiN Sample (Sr3-Sp4) with steel ball and TiN coated ball



Figure 14: TiN coating on aluminum substrate and inside of aluminum ring

Results and Discussion - MoS₂ film

Molybdenum disulphide (MoS₂) film was deposited by RF magnetron sputtering using a MoS₂ target. The film parameters were optimized and depositions were carried out with argon pressure maintained at 10 mTorr and forward power of 100 watt. The deposition time was 20 min resulting in film thickness in the range of 0.5-0.6 μm. Dektak Profilometry showed good thickness uniformity of MoS₂ films. Peel test showed good adhesion of MoS₂ coatings with glass substrates. Energy dispersive analysis of X-rays of MoS₂ films showed stoichiometric ratio of Mo and S (Atomic Percent Mo : S = 37.87:62.13) to form a MoS_{1.6} phase. Low friction values are obtained despite the MoS_y substoichiometry and an apparently random basal plane orientation, though this is not in contradiction with the literature where it is reported that stoichiometries above 1.2 are lubricating [36] and MoS₂ is able to preferentially re-orient under the action of friction with basal planes parallel to the sliding direction [37-38]. MoS₂ film as sputtered displays a black appearance and the surface appears to be very smooth and dense with fine grain structure. Scanning electron microscopy image of MoS₂ coatings (Figure 15) show that the grains are nanocrystalline in nature. The broad nature of peaks in X-ray diffraction patterns (Figure 16) confirmed the nanocrystalline nature of MoS₂ films.

The advantage is that the lubricating effect will be maintained throughout the entire lifetime because the lubricating species is available throughout the wearing of the entire thickness of the coating and the coating is hard and less likely to be removed by abrasive wear [39]. The MoS₂ film is removed during sliding and constitutes a source of lubricating particles that adhere to both the contracting bodies and limit the mating of the surfaces.

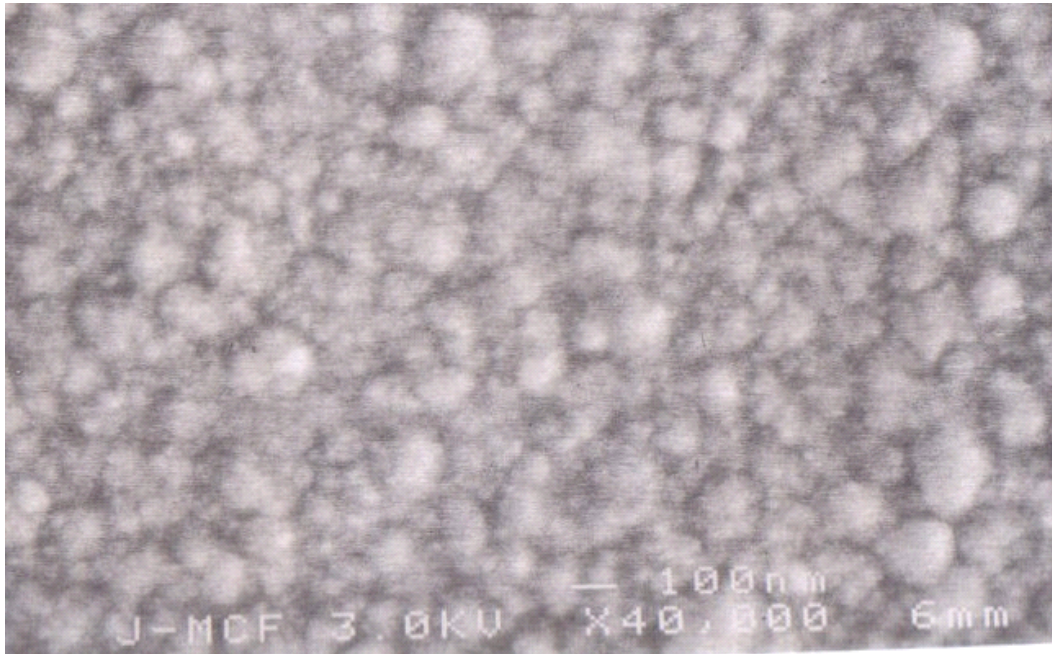


Figure 15: Scanning Electron Microscopy image of MoS₂ Coating

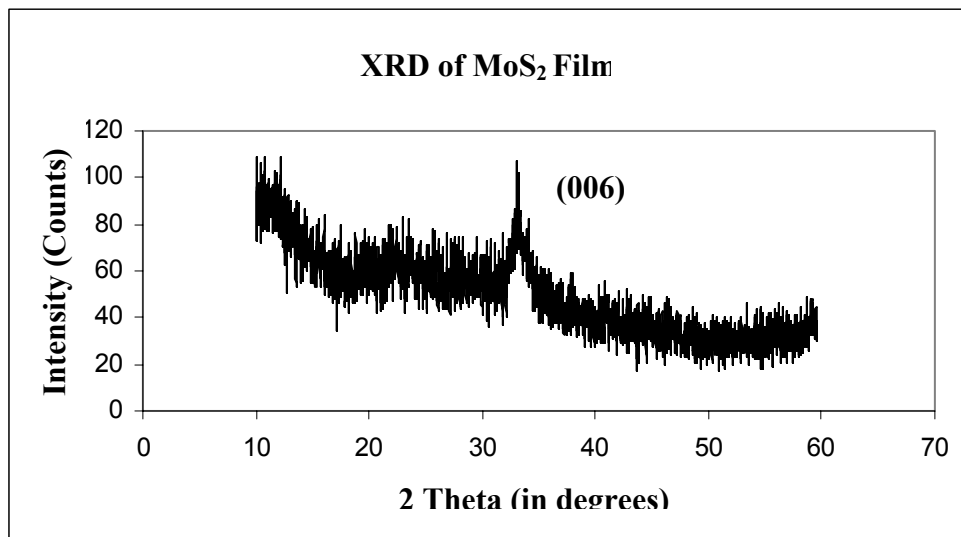


Figure 16: XRD Pattern of MoS₂ film

Results and Discussion – TiN/MoS₂ film

The bilayer coating of TiN/MoS₂ was deposited using the above optimized parameters for both the TiN and MoS₂ films. The microstructure of the film is determined by the deposition parameters. Therefore, the TiN film deposited is a multilayered film with a first layer of only Ti with Ar pressure maintained at 5 mTorr. This pure Ti layer is grown to assure a good bonding between the coating and substrate. The second layer of TiN is deposited at a forward power of 150 watt with the Ar pressure maintained at 5 mTorr and N₂ pressure maintained at 1 mTorr. The third layer of TiN is also deposited at a forward power of 150 watt with Ar pressure maintained at 1 mTorr and N₂ pressure maintained at 1 mTorr. MoS₂ film depositions were carried out with argon pressure maintained at 10 mTorr and forward power of 100 watt. The deposition time was 20 min resulting in film thickness in the range of 0.5-0.6 μm. Sample 3 and 4 from Table 6 consists of increased time of deposition for MoS₂ coating to increase the thickness of MoS₂ layer and study the effect on friction and wear properties of tribological films.

XRD pattern of the TiN/MoS₂ (Samp. 2) bilayer coating is shown in Figure 17. MoS₂ peak in the bilayer coating have oriented to the (002) plane from the earlier (006) plane in case of MoS₂ coated sample and can be attributed to the growth of MoS₂ film on top of the TiN film.

TEM Micrographs

The TEM micrographs of the TiN/MoS₂ (Samp. 2) bilayer coating are provided in Figures 18-24. Figure 18 shows the interface between Ti layer and the glass substrate. The interface between the coating and substrate appears to be good. Figure 19 shows the interface between the Ti layer and the glass layer at magnification of 390K. Ti layer appears to have a dense fibrous

microstructure. Figure 20 and Figure 21 shows the grains in Ti and TiN layer respectively at a magnification of 49K. The grains sizes are less than 100 nm. Figure 22 shows the interface between the Ti Layer to TiN layer at magnification of 98K and appears to be very good showing a continuation of growth. Figure 23 and Figure 24 shows the interface between the TiN layer to MoS₂ layer at a magnification of 115K and at a magnification of 390K respectively. The interface appears to be very good showing a continuation of growth.

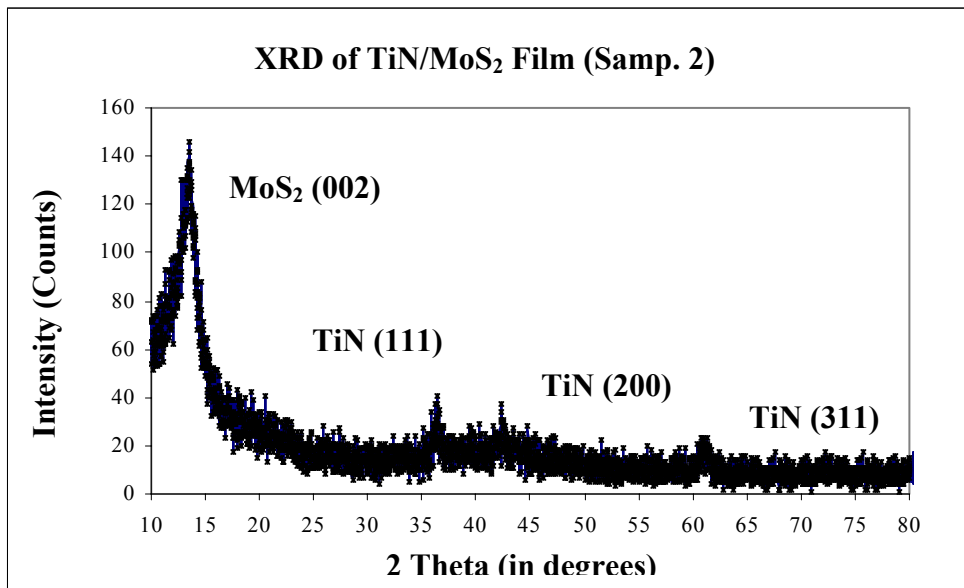


Figure 17: XRD Pattern of TiN/MoS₂ film (Samp. 2)

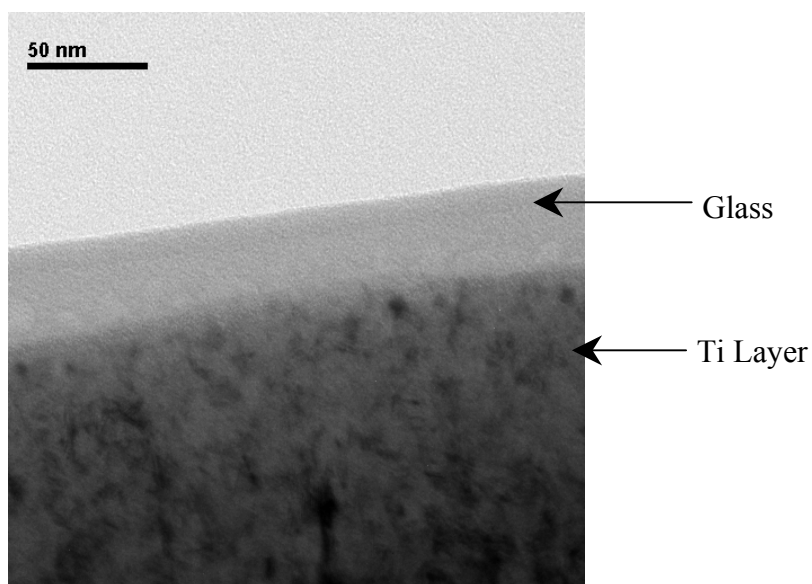


Figure 18: Interface – Glass to Ti Layer

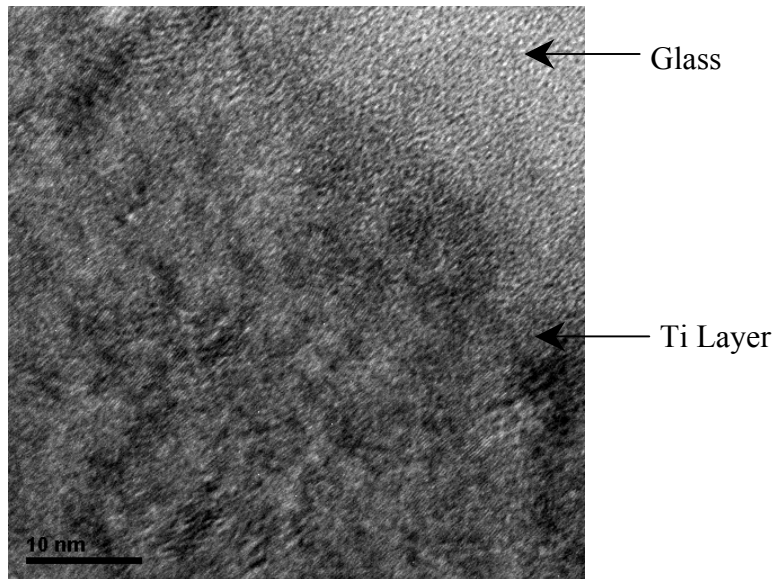


Figure 19: Interface – Glass to Ti Layer at magnification of 390K

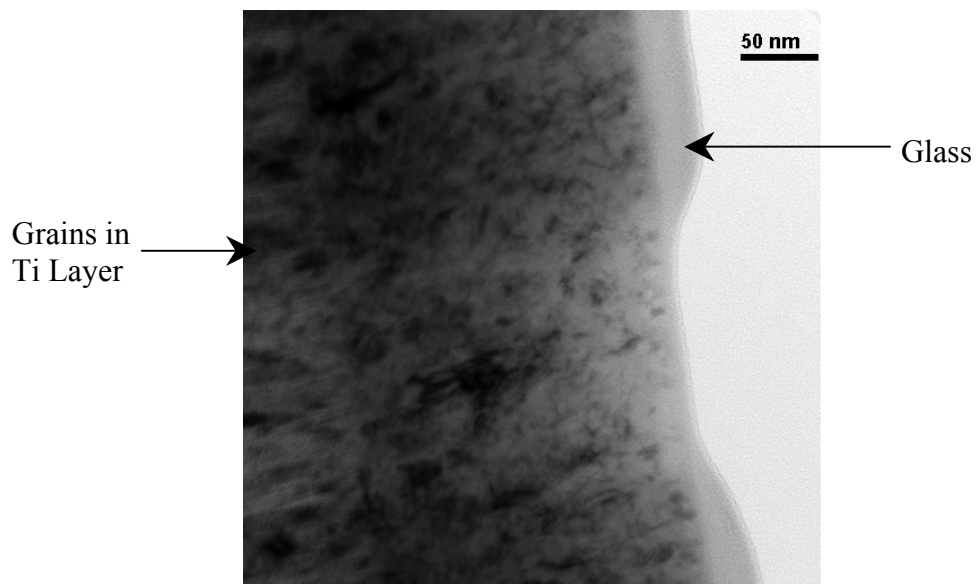


Figure 20: Grains in Ti layer at magnification of 49K

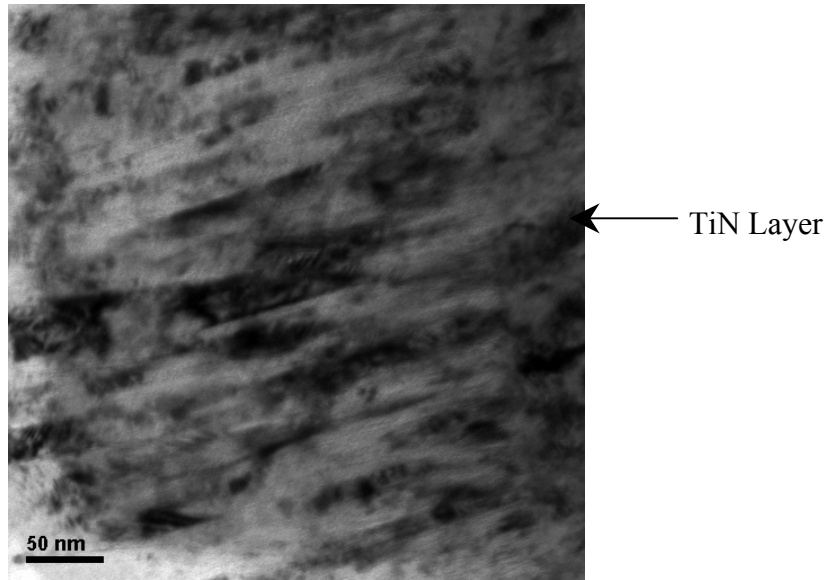


Figure 21: Grains in TiN layer at magnification of 49K

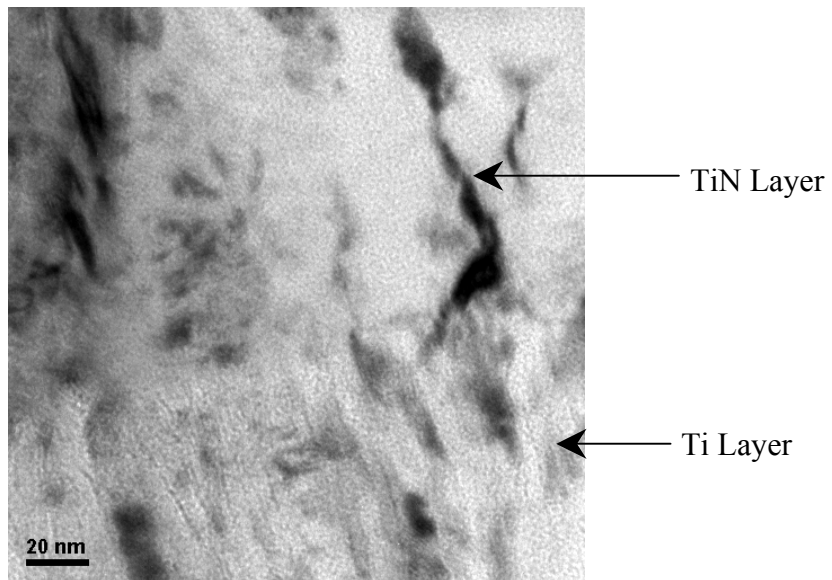


Figure 22: Interface - Ti Layer to TiN layer at magnification of 98K

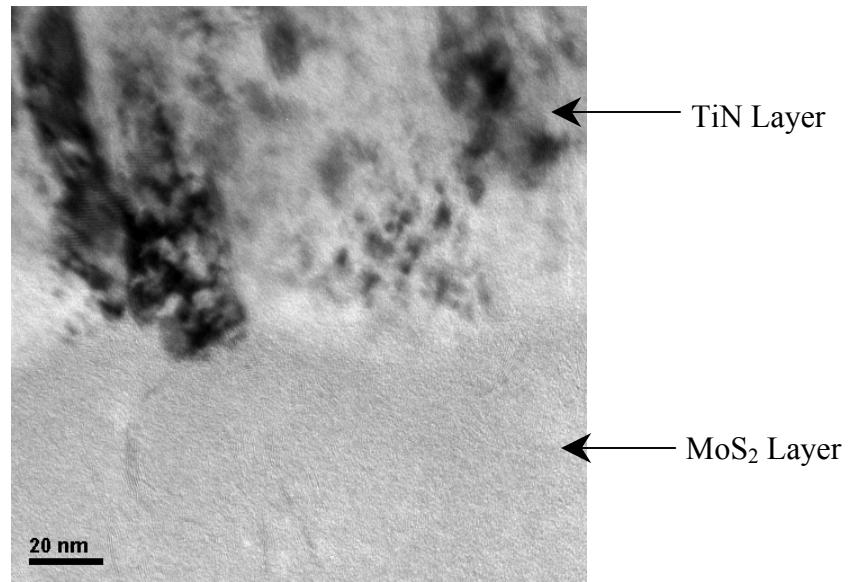


Figure 23: Interface - TiN layer to MoS₂ layer at magnification of 115K

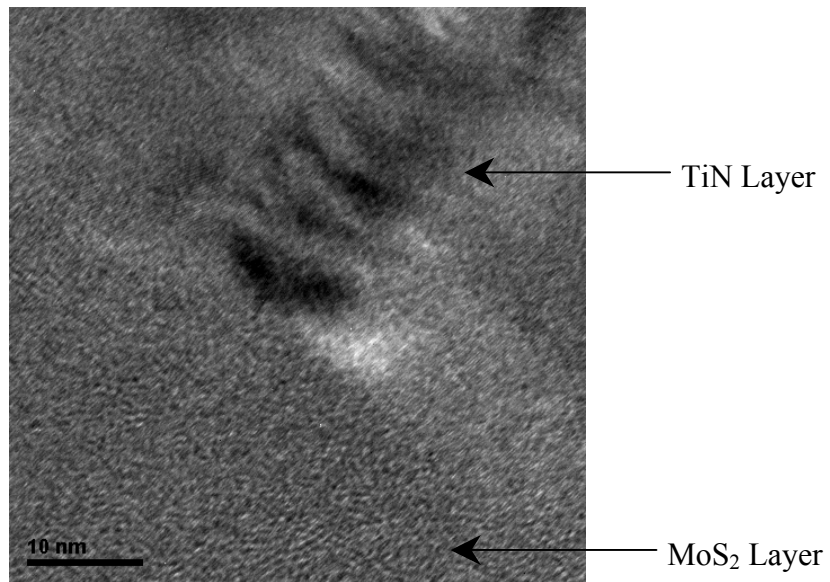


Figure 24: Interface - TiN layer to MoS₂ layer at magnification of 390K

Friction and Wear Tests of TiN/MoS₂ Samples.

The COF is not only an intrinsic property of a material but depends on a number of factors such as materials in contact, contact geometry, environment and surface conditions, temperature and method of deposition and the load parameters.

The coefficient of friction tests were carried out by ball-on-disc method at room temperature on TiN/MoS₂ sample (Samp. 1) on aluminum substrate with the assistance of Dr. Gregory Sawyer and his colleagues at University of Florida and are provided in Table 11.

The coefficient of friction measurements on TiN/MoS₂ (Samp. 2 deposition parameters) bilayer coating on Si wafer were carried out at room temperature on the “Tytron™ 250 MicroForce Testing Equipment” with the assistance of Dr. Quanfang Chen and his colleagues at UCF. These measurements require the film to be deposited on three 0.9 mm diameter bumps on 1 cm x 1 cm silicon wafer to minimize the contact and providing more accurate coefficient of friction and wear measurements. TiN/MoS₂ film with optimized deposition parameters same as Samp. 2 were deposited on 1 cm x 1 cm silicon wafers with and without these bumps for the friction and wear measurements. Figure 25 shows optical microscopy image of TiN/MoS₂ film on Si-wafer. Number of measurements were carried out and the average coefficient of friction (Figure 26) for the TiN/MoS₂ Bilayer coating on Si wafer with 1 N normal load was = 0.045. Initial friction maxima are often associated with transfer film formation.

Table 11: Summary of friction tests by ball-on-disc and pin-on-disc method on Series-3 TiN films

Substrate	Tribological Coating	Coating Pair	Force (gm)	Speed (RPM)	Average COF
Aluminum	TiN/MoS ₂	3/16 diam alumina ball	66.3	605	0.205

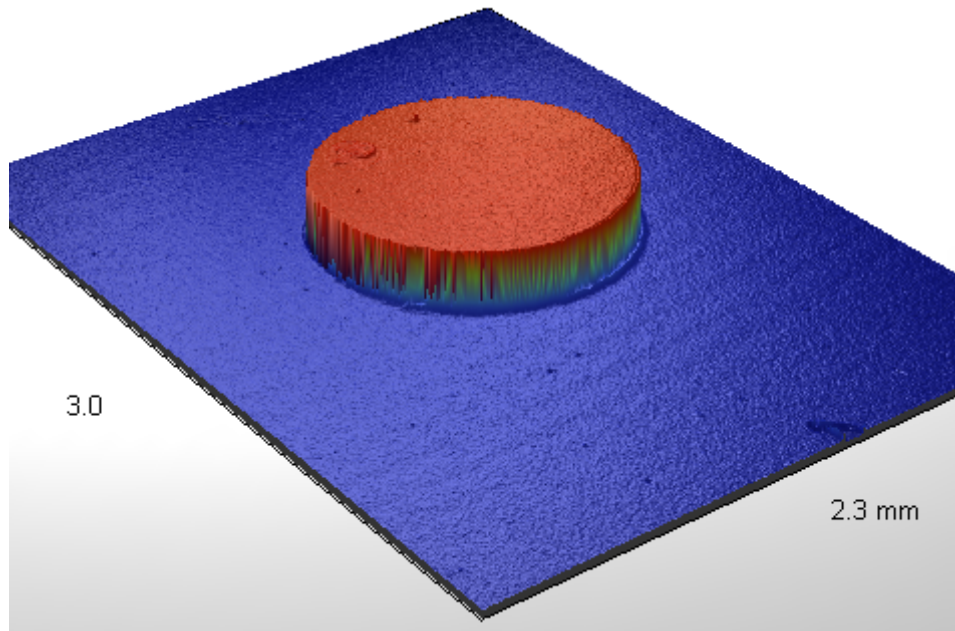


Figure 25: Optical Microscopy image of TiN/MoS₂ film on bumps on Si-wafer

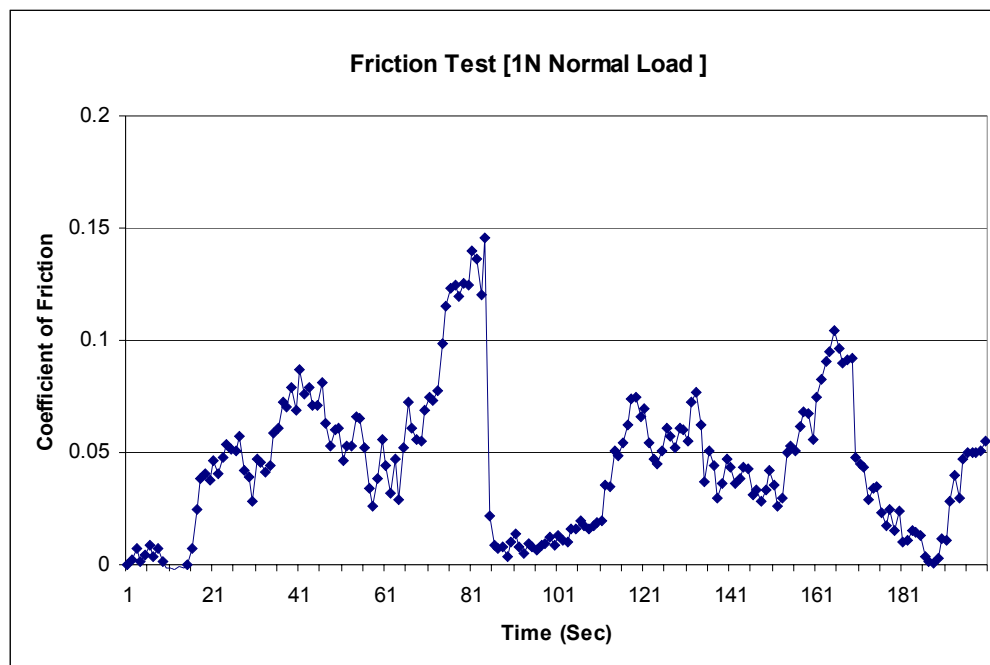


Figure 26: Friction test of TiN/MoS₂ Sample (Samp. 2 dep. Conditions) on Si-wafer

Friction tests were also carried on TiN/MoS₂ samples (Samp. 1, Samp. 2, Samp. 3, & Samp. 4) out at University of South Florida with the assistance of Dr. Kumar and his colleagues by pin-on-disc method. The summary of the friction tests is shown in Table 12. The summary of the wear tests on TiN/MoS₂ samples is shown in Table 13. Both friction and wear tests were carried out at room temperature. Figure 27-29 provides the friction tests on TiN/MoS₂ samples on glass substrate (Samp. 1, Samp. 2, Samp. 3, & Samp. 4) by pin-on-disc method. Figure 30-32 provides the wear tests on TiN/MoS₂ samples on glass substrate (Samp. 1, Samp. 2, Samp. 3, & Samp. 4) by pin-on-disc method. Both friction and wear tests shows that the coating provided low friction and good wear resistance.

The friction tests were carried out at room temperature with an average force of 50 gm exerted by the ball on the coating and the ball traveled a total distance of 40 mm with a sliding velocity of 0.2 mm/sec. The exerted force was adjusted at 50 gm in consultation with Mr. Krishna and speed was limited by the instrument.

The coefficient of friction values on TiN/MoS₂ samples with various coating pairs: uncoated, TiN coated, TiN/MoS₂ coated steel balls by pin-on-disc method on glass and aluminum substrates were comparable to each other and were in the range of 0.08 – 0.225 as can be seen from Table 12. Frictional values tended to follow a complex series of changes before reaching a steady state condition. MoS₂ between contact surfaces provides good lubrication and the friction curves clearly indicated that the addition of MoS₂ film have a dramatic effect on the friction coefficient.

Samp. 1 and Samp. 2 with only single layer of MoS₂ coating on both Aluminum and glass substrates provided the lowest values by both the ball-on-disc and pin-on-disc methods. Samp. 3 and Samp. 4 with two layers of MoS₂ coating provided higher coefficient of friction and wear

values. Also the TiN coated steel ball produced the lowest friction as compared to the bare steel ball as well as TiN/MoS₂ coated steel ball. The TiN/MoS₂ coated sample Samp2. produced the lowest average friction coefficient of 0.08 with TiN coated steel ball and also had lowest friction results with all balls as compared to Samp. 3 and Samp. 4. Wear tests indicate that TiN/MoS₂ coated balls provide low friction over increased time as compared to TiN coated balls. Friction values over longer cycles do not seem to increase showing good wear resistance of the coating. Increasing the deposition time and thickness for MoS₂ film on the bilayer coating samples do not seem to reduce friction. Optimized hardness and friction values obtained for Samp. 2 overall provides good friction and wear resistance.

Table 12: Summary of Friction Tests

Samp.#	Trib. Coating	Coating Pair	Subs.	Force (gm)	Cycles #	COF Range	Average COF
Samp 1	TiN / MoS ₂	Steel Ball	Al	50		0.10 - 0.18	0.14
Samp 2	TiN / MoS ₂	Steel Ball	Glass	50		0.12 - 0.20	0.16
Samp 3	TiN / MoS ₂	Steel Ball	Glass	50		0.15 - 0.17	0.16
Samp 4	TiN / MoS ₂	Steel Ball	Glass	50		0.20 - 0.25	0.225
Samp 1	TiN / MoS ₂	TiN coated Steel Ball	Al	50		0.15 - 0.18	0.165
Samp 2	TiN / MoS ₂	TiN coated Steel Ball	Glass	50		0.06 - 0.10	0.08
Samp 3	TiN / MoS ₂	TiN coated Steel Ball	Glass	50		0.18 - 0.20	0.19
Samp 4	TiN / MoS ₂	TiN coated Steel Ball	Glass	50		0.18 - 0.20	0.19
Samp 2	TiN / MoS ₂	TiN / MoS ₂ coated Steel Ball	Glass	50		0.15 - 0.20	0.175
Samp 3	TiN / MoS ₂	TiN / MoS ₂ coated Steel Ball	Glass	50		0.15 - 0.20	0.175
Samp 4	TiN / MoS ₂	TiN / MoS ₂ coated Steel Ball	Glass	50		0.18 - 0.20	0.19

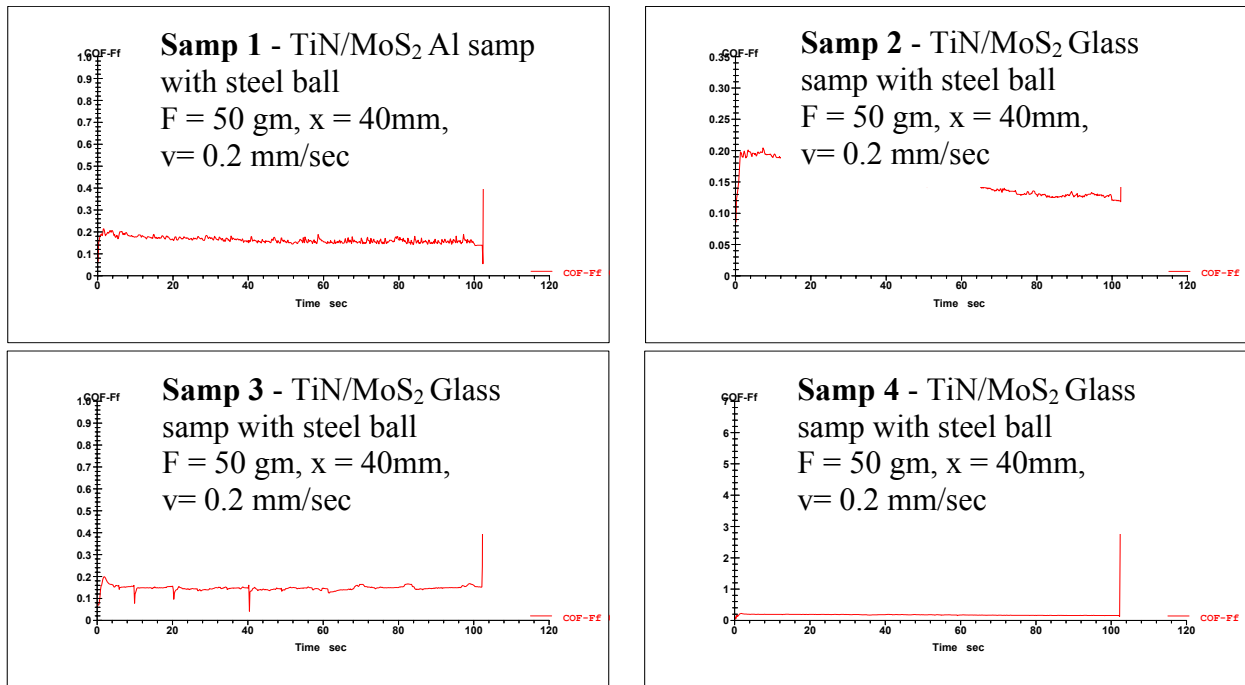


Figure 27: Friction test of TiN/MoS₂ Samples with steel ball

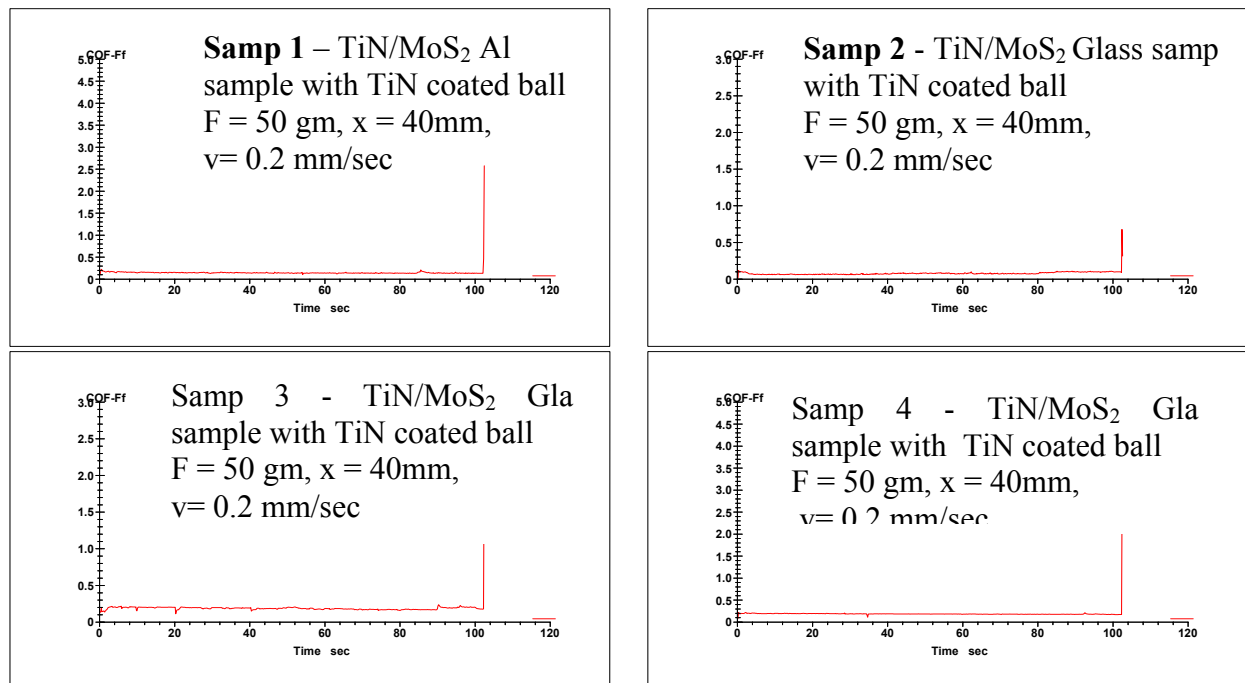


Figure 28: Friction test of TiN/MoS₂ Samples with TiN coated steel ball

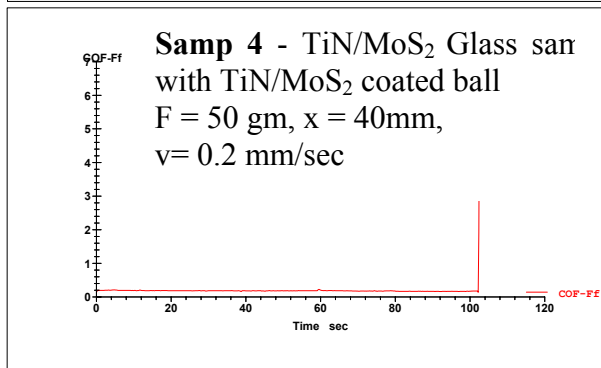
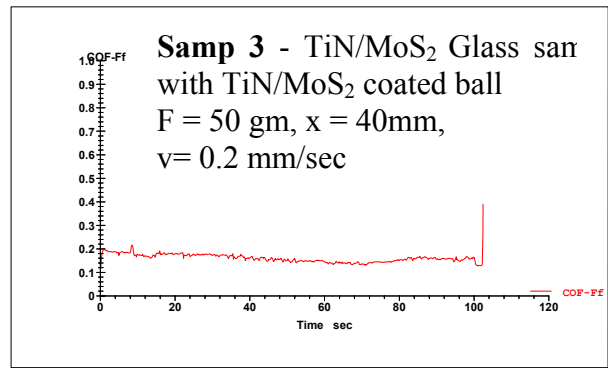
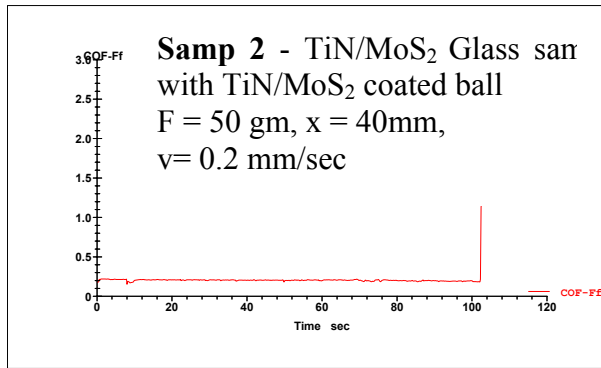


Figure 29: Friction test of TiN/MoS₂ Samples with TiN/MoS₂ coated steel ball

Table 13: Summary of Wear Tests

Samp.#	Trib. Coating	Coating Pair	Subs.	Force (gm)	Cycles #	COF Range	Average COF
Samp 1	TiN / MoS ₂	Steel Ball	Al	50	300	0.15 - 0.21	0.18
Samp 2	TiN / MoS ₂	Steel Ball	Glass	50	300	0.15 - 0.20	0.175
Samp 3	TiN / MoS ₂	Steel Ball	Glass	50	300	0.25 - 0.30	0.275
Samp 4	TiN / MoS ₂	Steel Ball	Glass	50	300	0.20 - 0.25	0.225
Samp 2	TiN / MoS ₂	TiN coated Steel Ball	Glass	50	300	0.22 - 0.28	0.25
Samp 3	TiN / MoS ₂	TiN coated Steel Ball	Glass	50	300	0.25 - 0.31	0.28
Samp 4	TiN / MoS ₂	TiN coated Steel Ball	Glass	50	300	0.25 - 0.35	0.30
Samp 2	TiN / MoS ₂	TiN / MoS ₂ coated Steel Ball	Glass	50	300	0.20 - 0.25	0.225
Samp 3	TiN / MoS ₂	TiN / MoS ₂ coated Steel Ball	Glass	50	300	0.22 - 0.25	0.235
Samp 4	TiN / MoS ₂	TiN / MoS ₂ coated Steel Ball	Glass	50	300	0.25 - 0.30	0.275

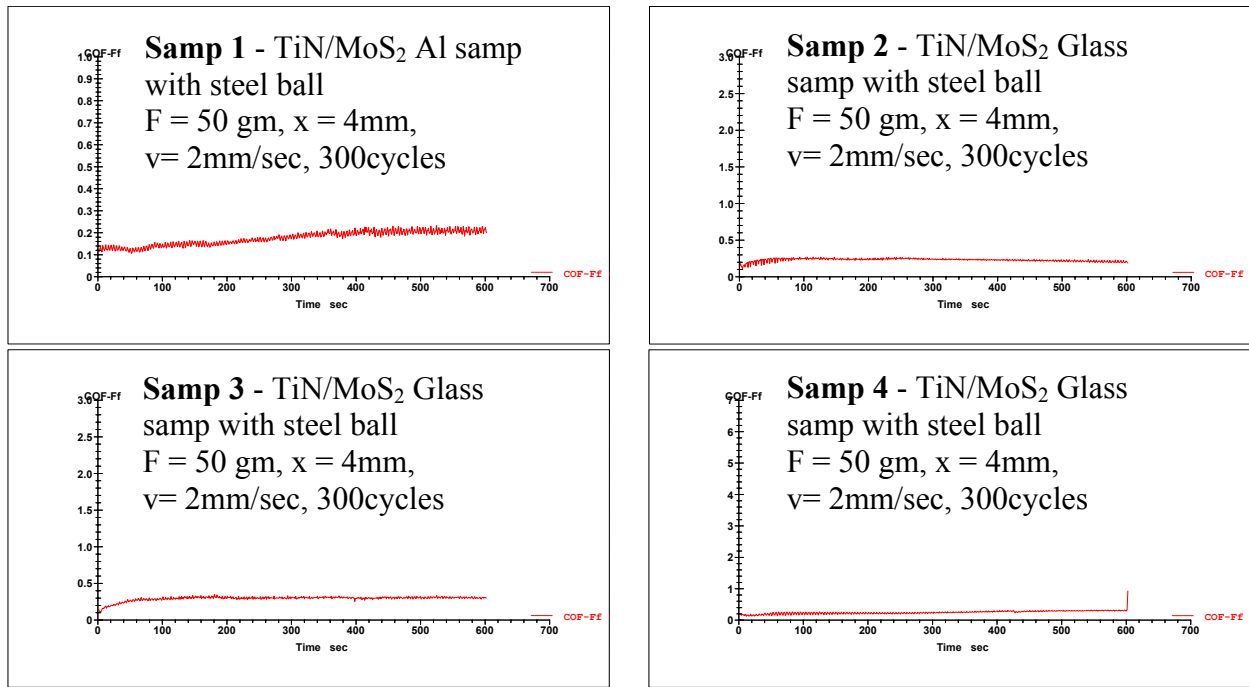


Figure 30: Wear test of TiN/MoS₂ Samples with steel ball

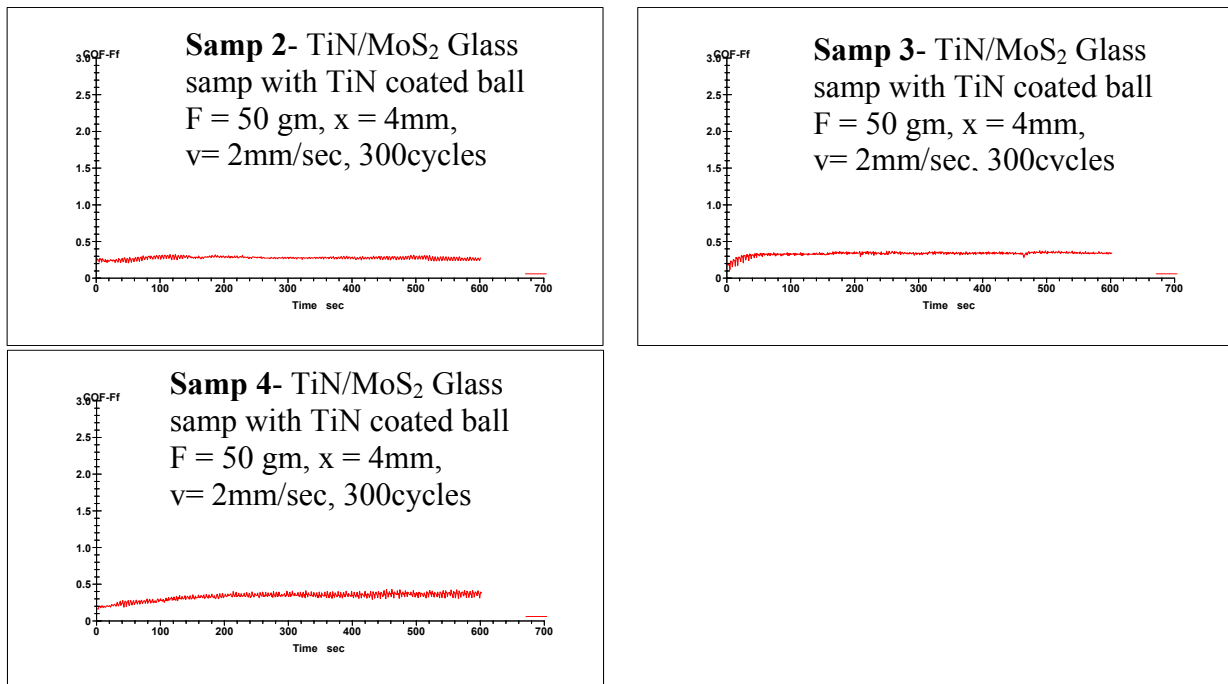


Figure 31: Wear test of TiN/MoS₂ Samples with TiN coated steel ball

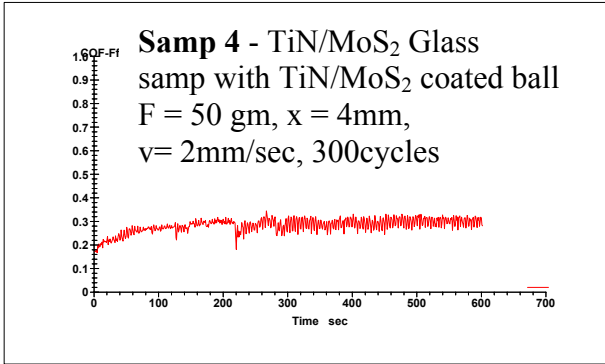
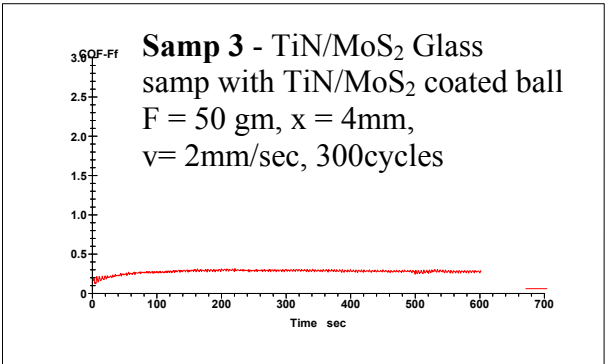
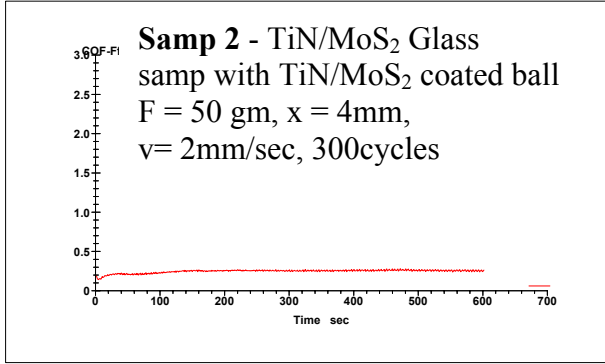


Figure 32: Wear test of TiN/MoS₂ Samples with TiN/MoS₂ coated steel ball

DIAMOND-LIKE CARBON FILM

Introduction

DLC films that are being used for tribological applications can also be employed for other applications such as protective coatings on the rear of solar cells replacing the components such as encapsulant and protective sheets on that side.

Amorphous DLC forms a large group of coatings. They can be doped with metals, nitrides and carbides to further improve the mechanical and tribological properties and to enhance the adhesion to the substrate. Under suitable conditions, DLC can provide a combination of good wear and corrosion resistance and a low friction [12]. DLC can be deposited by microwave assisted chemical vapor deposition process (MWCVD) [16]. Microwave assisted chemical vapor deposition (MWCVD) technique was chosen for preparation of DLC coatings due to advantages of microwave excited plasmas: higher degree of ionization, wide operating pressure range, high electron to gas temperature ratio and absence of electrodes. DLC coatings are being prepared and analyzed for their microstructure-properties relationship.

DLC films are constituted by an amorphous carbon network with a mixture of graphitic type bonding (sp^2) and diamond type tetragonal bonding (sp^3) carbon hybridizations, some hydrogenated amorphous carbon (a-C:H) films containing up to 50 at% hydrogen, others such as amorphous carbon (a-C) containing less than 1 at% hydrogen. The “DLC” terminology is commonly used to designate the hydrogenated form of amorphous carbon films, in spite of containing sp^3 fraction generally smaller than 50%. DLC may be divided into four categories, the amorphous carbon (a-C), hydrogenated amorphous carbon (a-C:H), tetrahedral amorphous carbon (ta-C) and hydrogenated tetrahedral amorphous carbon (ta-C:H). The structure, properties and

tribological behavior of DLC films are dependent on the deposition process, the hydrogen concentration and chemical bonding in the film.

Pulsed laser deposition (PLD) produces tetrahedral amorphous carbon (ta-C) films similar to those from the mass selected ion beam deposition (MSIB) and filtered cathodic vacuum arc (FCVA) methods. Therefore, the most popular laboratory deposition method for DLC is RF plasma enhanced chemical vapor deposition (PECVD) [40]. For DLC deposition, the plasma should be operated at the lowest possible pressure, in order to maximize the ion to radical fraction of the plasma. However, even at 50 mTorr pressure, the ions are only about 10% of the film-forming flux. The ions can lose energy by collisions when being accelerated across the sheath. The ion energy is then no longer the sheath voltage. It is desirable to use a low pressure to minimize these collisions, to maintain a narrow ion energy distribution. However, this is not possible for conventional PECVD as the plasma will no longer strike. Lower pressure plasma can be created by using a magnetic field to confine the plasma, to increase the electron path length and increase the ionization efficiency. In microwave plasma CVD, the ionization energy is provided by very high frequency such as 2.45 GHz. At such frequencies, discharges have plasma density of $\sim 10^{10}/\text{cm}^3$. When hydrocarbon gases are decomposed in a discharge operated at frequencies in the range from dc to GHz, a hydrogenated form of amorphous carbon is produced. Microwave discharges have an advantage over DC and RF due to their inherent superiority in terms of quality of discharge. Some of the advantages of the microwave excited plasmas are: higher degree of ionization, wide operating pressure range, high electron to gas temperature ratio and absence of electrodes.

The coefficients of friction, $-\mu-$ for ta-C and ta-C:H are different. For a-C:H, coefficient of friction depends strongly on the relative humidity. Values of coefficient of friction below 0.05 are

found in vacuum and at low humidity. It increases to 0.1–0.15 when the humidity rises to normal atmospheric values of 30% and increases strongly at high humidity. In situ studies have shown that the higher values of coefficient of friction arise from the water, not oxygen in the atmosphere [40].

The diamond surface is normally inert because its broken bonds are generally passivated by C-H bonds. This means that diamond surfaces are hydrophobic, closed-shell bonded systems, and they will only contact through van der Waals forces. Under pressure, the contact will be elastic. As the contact shears, it will break at the weaker van der Waals bonds, not the bulk C-C bonds, so the friction force has an adhesive/deformation nature rather than abrasive. The hydrophobic nature of DLC is important since an interlayer of water will also provide adhesive contact. Therefore, super-low friction is correlated with hydrogen saturation across the shearing plane through weak van der Waals interactions between the flexible hydrocarbon chains located on the two contacting surfaces.

The amorphous hydrogenated carbon (a-C:H) behaves in this manner under vacuum or low humidity. Contact with a different surface causes a transfer layer of a-C:H to be formed on the other surface. Thus, the contact is between two basically similar hydrophobic a-C:H surfaces, and the friction coefficient is very low. High humidity is believed to interfere with the formation of the contact layer, and cause it to become oxidized/hydrated, so that it no longer forms the van der Waals bonds. If the transfer layer does not form, the counter surface is no longer hydrophobic, and the friction coefficient is much higher.

The ta-C has a larger coefficient of friction than a-C:H in vacuum of about 0.1 to 0.15. Intercalation of water between the graphite layers lowers the friction coefficient and thus, the coefficient of friction for ta-C decreases with increasing humidity [40].

Experimental Technique

The MWCVD system that was designed and constructed in-house is shown in Figure 33. Initial deposition and characterization of diamond-like-carbon (DLC) coatings is being carried out using this setup. The components of this system have been procured from Gerling Applied Engineering Inc. It uses a 1.2 KW, 2.45 GHz magnetron head (Model GA4001) powered by a switching power generator (Model SM445G). The microwave energy is launched into the waveguide WR284 from the magnetron source. The other components in the setup are a three port circulator (Model GA1105) and a short water cooled dummy load (Model GA1204), directional waveguide couplers (Model GA310X) to extract the signals for measurements of the forward and reflected power using a Agilent E44118B Power meter and a Agilent 8481A power sensor, a four stub waveguide tuner for matching the load impedance (each stub is $\lambda_g/4$ wavelength apart to be able to generate an impedance of any value at any phase), a downstream plasma applicator (Model GA610x) to bring the plasma into the chamber and a sliding short circuit (Model GA1205) for providing the reflecting surface for the incident microwave radiations so that the Q of the plasma cavity can be increased to get the gas breakdown by the movement of the sliding short. The plasma applicator is a quartz tube. Microwave leakage was checked using an ETS Lindgren HI-1501 microwave survey meter. The reflected power was reduced by empirically adjusting the four stub tuners and position of the sliding short. These adjustments also resulted in plasma uniformity over the substrate surface used for depositing the coatings.

An unbiased (Stainless Steel foil - 127 μm and Si-wafer) as well as biased stainless steel substrates were used for depositing the DLC films. The processing gases were a mixture of Ar, precursor methane (CH_4) and hydrogen (H_2) gases. The processing gases are fed into the tube from the top. The bottom of the plasma applicator is connected to a 15.24 cm six-way cross vacuum

chamber pumped with a turbomolecular pump-mechanical pump combination. The chamber was evacuated to a base pressure of $<10^{-5}$ Torr and the microwave plasma was generated with the application of 150 watt and 300 watt of microwave power and using argon as a carrier gas. After stabilization of the plasma, precursor gases CH_4 and H_2 was introduced. A gate valve control system is used for throttling and adjusting the gas pressure to the required operating pressures.



Figure 33: Microwave CVD setup

Results and Discussion

DLC films have been prepared on unbiased (Stainless Steel foil - 127 μm and Si-wafer) as well as biased stainless steel substrate at (-150V). Based on our discussions with Professor Jean Michel Martin and his group at University Institute of France, Lyon, France, the possibility of analyzing the samples by forward recoil elastic Rutherford backscattering for hydrogen content was discussed. Tribological measurements are also being planned at University of Florida.

Among the different types of diamond-like carbon coatings, hydrogenated amorphous carbon films have the characteristic of exhibiting superlow friction under ultra-high vacuum or in inert environments. However, not all hydrogenated amorphous carbon films lead to superlow friction. When slid in high vacuum, the friction coefficients of these films stabilizes either at very low or high value as reported in various studies. However, literature shows that DLC films containing large amounts of hydrogen reached friction coefficients near 0.01 in vacuum whereas films with low hydrogen content reached values higher than 0.35. Literature shows that hydrogen is responsible for an ultra-low friction level through repulsive dipole interactions of C-H bonds on the surfaces of both counterfaces.

The strong difference observed under ultra-high vacuum between high and low friction films could be explained by surface interactions between the carbon-covered counterfaces. For higher hydrogen content in the film, the surface is covered by hydrogen atoms, leading to weak Van-der-Waals interactions between the sliding surfaces, whereas for lower hydrogen content, there are not enough hydrogen atoms to shield the strong interactions between the π orbitals of sp^2 carbon double bonds. Moreover, some references also demonstrate that high friction under ultra-high vacuum, can be altered by the introduction of gaseous hydrogen, which enabled the

achievement of superlow friction, probably by promoting tribochemical reactions between hydrogen and the a-C:H surface. Thus, the lubricating role of hydrogen on a-C:H surface is now commonly accepted, with weak Van-der-Waals interactions accounting for the superlow friction values.

Continuing progress of diamond-like carbon films is dependent on special characterization techniques to analyze their properties, such as, the hydrogen and impurity content of the films as it can affect both the film integrity and its properties. The following important techniques are described in detail in addition to Fourier transform infrared spectroscopy and Ellipsometry:

- Elastic recoil detection spectroscopy (ERD) is used to measure the Hydrogen concentration of the film which is related to the growth parameters and the quality of the film. It is a fast and non-destructive method of obtaining H profiles up to depths of about 600 nm. In this method, a beam of MeV energy light ions, for example He⁺ is directed at the target causing a small fraction of the H atoms in the target to be ejected by elastic recoil collisions. The concentration of H atoms versus depth in the target can be calculated from the observed energy spectra of the recoiled H atoms using standard kinematic analysis.
- Raman scattering can be used for nondestructive evaluation of the quality of a diamond film, as the dominant zone-center vibrational mode frequencies of diamond (1332 cm⁻¹), graphite (1589 cm⁻¹), and disordered carbon (1360 cm⁻¹) are easily distinguished.
- Hysitron Triboindenter is a depth sensing indentation device capable of nanometer displacement resolution and micro-Newton loads. In-situ imaging of indents is possible with a CCD camera and a piezo scanning probe feature. Test modes include nanoindentation, nanoscratch and nanowear. Literature from the past 10 years contains extensive amounts of nanoindentation studies, however, nanoscratch and nanowear are relatively new. Nanoscratch

testing mode can provide a relative study of coating adhesion. Nanowear testing can provide a pin on flat rastering wear test, but friction coefficients are not measured.

These coatings will be analyzed at the National Renewable Energy Laboratory (NREL) by the following techniques: Raman spectroscopy, Fourier transform infrared spectroscopy and Ellipsometry. ERD will be carried out at the University of North Carolina and tribological measurements with Hysitron triboindenter will be carried out at the University of Florida.

CONCLUSIONS

Hydrogen production at present is mostly from fossil sources. It is a clean, sustainable form of carrier of energy used in mobile and stationary applications. Solar photoelectrochemical processes are being developed for hydrogen production. Hydrogen storage is done in three main ways: in compressed form, liquid form and by chemical bonding. Near term spaceport operations are one of the prominent applications for usage of large quantities of liquid hydrogen as a cryogenic propellant. Efficient storage and transfer of liquid hydrogen is essential for reducing the launch costs. Efficiency of the cryocooler being developed for distributed cooling of liquid hydrogen systems for spaceport applications depends mainly on friction and wear between the mating parts. Tribological coatings will help reduce friction and wear resulting in improved efficiency of the cryocooler.

Dense well adherent coatings of TiN/MoS₂ were obtained. Scanning electron microscopy images and broad nature of peaks in X-ray diffraction patterns of both TiN and MoS₂ coatings show that the grains are nanocrystalline in nature. These composite coatings containing the hard ceramic matrix phase of TiN with microhardness value of 24.90 GPa and average elastic modulus value of 256.60 GPa and a solid lubricating phase of MoS₂ provided low friction values. The coefficient of friction values by ball-on-disc method for TiN and TiN/MoS₂ coatings on glass and aluminum substrates with various coating pairs (TiN, TiN/MoS₂ coated steel ball, average force of 50 gm) were in the range of 0.08 – 0.2. MoS₂ between contact surfaces provides good lubrication and the friction curves clearly indicated that the addition of MoS₂ film have a dramatic effect on the friction coefficient. The values of hardness and coefficient of friction were comparable or better than those of commercial tribological coatings.

Samp. 1 and Samp. 2 with only single layer of MoS₂ coating on both Aluminum and glass substrates provided the lowest values by both the ball-on-disc and pin-on-disc methods. Samp. 3 and Samp. 4 with two layers of MoS₂ coating provided higher coefficient of friction and wear values. Also the TiN coated steel ball produced the lowest friction as compared to the bare steel ball as well as TiN/MoS₂ coated steel ball. The TiN/MoS₂ coated sample Samp2. produced the lowest average friction coefficient of 0.08 with TiN coated steel ball and also had lowest friction results with all balls as compared to Samp. 3 and Samp. 4. Wear tests indicate that TiN/MoS₂ coated balls provide low friction over increased time as compared to TiN coated balls. Friction values over longer cycles do not seem to increase showing good wear resistance of the coating. Increasing the deposition time and thickness for MoS₂ film on the bilayer coating samples do not seem to reduce friction. Optimized hardness and friction values obtained for Samp. 2 by selecting suitable composition and deposition parameters overall provides good friction and wear resistance.

MWCVD system for deposition of DLC coatings was designed and fabricated. Initial deposition and characterization of DLC coatings are being carried out.

Future work will address the endurance issues of these coating at the cryogenic temperatures.

REFERENCES

- [1] J. Meneve, K. Vercammen, E. Dekempeneer, J. Smeets, *Surface and Coatings Technology*, Vol. 94-95, 1997, pp. 476-482.
- [2] K. Taube and K. Bewilogua, *Encyclopedia of Materials: Science and Technology*, 2003.
- [3] K Holmberg and A Matthews, *Coatings Tribology*,. Tribology Series - 28, Elsevier, 1994.
- [4] J L Vossen and W Kern, *Thin Film Processes II.* , Academic Press, 1991.
- [5] J A Thornton, *Journal of Vacuum Science and Technology*, No. 11, 1974, pp. 666–670.
- [6] C Donnet, *Condensed Matter News* 4, 1996, pp. 9–24.
- [7] S. Hogmark, S. Jacobson, O. Vingsbo, *Friction Lubrication and Wear Technology*, ASM Handbook, Vol. 18, 1992, pp. 176.
- [8] A. S. Korhonen, *Vacuum*, No. 45, Iss.10-11, 1994, pp. 1031-1034.
- [9] D. Drees, J. P. Celis, E. Dekempeneer and J. Meneve, *Surface Coatings and Technology*, Vol. 86-87, 1996, pp. 575-580.
- [10] R. Thom, L. Moore, W. D. Sproul and T. Peter Chang, *Surface and Coatings Technology*, Vol. 62, Iss. 1-3, 1993, pp. 423-427.
- [11] T. Gries, and B. Wulfhorst, *Surface and Coatings Technology*, Vol. 68-69, 1994, pp. 500–506.
- [12] S. Hogmark, S. Jacobson, and M. Larsson, *Wear*, Vol. 246, Iss. 1-2, 2000, pp. 20-33.
- [13] D. S. Rickerby and S.J. Bull, *Surface and Coatings Technology*, Vol.. 39-40, 1989, pp. 315-328.
- [14] U. Helmersson, J. E. Sundgren and J.E. Greene, *Journal of Vacuum Science and technology* A4, 1986, pp. 500-504.
- [15] R. F. Bunshah and C. V. Deshpandey, *Vacuum*, Vol. 39, No. 10, 1989, pp. 955-965.
- [16] D. S. Patil, K. Ramachandran, N. Venkatramani, M. Pandey and R. D’Cunha, *Pramana Journal of Physics*, Vol. 55, Nos. 5 & 6, 2000, pp. 933-939.
- [17] L. J. Meng, A. Azevedo, and M. P. dos Santos, *Vacuum*, Vol. 46, 1995, pp. 233-239.
- [18] M. Zlatanovic, R. Belosevac, N. Popovic, and A. Kunosic, *Surface and Coatings Technology*, Vol. 106, 1998, pp. 150-155.
- [19] A. J. Perry, *Journal of Vacuum Science Technology A*, Vol. 8, No. 3, 1990, pp. 1351-1358.
- [20] S. Wilson, and A.T. Alpas, *Surface and Coatings Technology*, Vol. 108-109, 1998, pp. 369-376.
- [21] J. Deng, M. Braun, and Y. Wei, *Journal of Vacuum Science Technology A*, Vol. 16, No. 4, 1998, pp. 2073-2077.

- [22] S.W. Huang, M.W. Ng, M. Samandi, and M. Brandt, *Wear*, Vol. 252, Iss. 7-8, 2002, pp. 566-579.
- [23] X. He, N. Baker, B. A. Kehler, K. C. Walter, and M. Nastasi, *Journal of Vacuum Science Technology A*, Vol. 18, No. 1, 2000, pp. 30-36.
- [24] P. Hones, M. Diserans, R. Sanjines, and F. Levy, *Journal of Vacuum Science and Technology B*, Vol. 18, No. 6, 2000, pp. 2851-2856.
- [25] Y. Liu, A. Erdemir, and E.I. Meletis, *Surface and Coatings Technology*, Vol. 82, 1996, pp. 48-56.
- [26] A. Vanhulsel, B. Blanpain, J. P. Celis, and J. Roos, E. Dekempeneer, J. Sneets, *Surface and Coatings Technology*, 98 (1998), pp. 1047-1052.
- [27] S. Zhang, B. Wang, and J. Y. Tang, *Surface Engineering*, Vol. 13, No. 4, 1997, pp. 303-309.
- [28] S. A. Catledge, and Y. K. Vohra, *Journal of Applied Physics*, Vol. 78, No. 12, 1995, pp. 7053-7058.
- [29] D. M. Bhusari, J. R. Yang, T. Y. Wang, S. T. Lin, K. H. Chen, and L. C. Chen, *Solid State Communications*, Vol. 107, No. 6, 1998, pp. 301-305.
- [30] R. Stockel, K. Janischowsky, S. Rohmfeld, J. Ristein, M. Hundhausen, and L. Ley, *Diamond and Related Materials*, Vol. 5, 1996, pp. 321-325.
- [31] Y. W. Bae, W. Y. Lee, T. M. Besmann, C. S. Yust, and P. J. Blau, *Material Science and Engineering A*, Vol. 209, 1996, pp. 372-376.
- [32] W. G. Moffatt, *Binary Phase Diagrams Handbook*, 1984.
- [33] E. Vogelzang, J. Sjollem, H. J. Boer, and J. Th. M. De Hosson, *Journal of Applied Physics*, Vol. 61, 1987, pp. 4606-4611.
- [34] J. E. Sundgren, *Thin Solid Films*, Vol. 128, 1985, pp. 21-44.
- [35] R. Gilmore, M. A. Baker, P. N. Gibson, W. Gissler, M. Stoiber, P. Losbichler, and C. Mitterer, *Surface and Coatings Technology*, Vol. 108-109, Iss. 1-3, 1998, pp. 345-351.
- [36] M. Larsson, M. Bromark, P. Hedenqvist and S. Hogmark, *Surface and Coatings Technology*, Vol. 76-77, 1995, pp. 202-207.
- [37] J. Moser, F. Levy and F. Bussy, *Journal of Vacuum Science & Technology A*, Vol. 12, Iss. 2, 1994, pp. 494-500.
- [38] T. Le Mogne, C. Donnet and J.M. Martin, *Journal of Vacuum Science & Technology A*, Vol. 12, Iss. 4, 1994, pp. 1998-2004.
- [39] R. Goller, P. Torri, M. A. Baker, R. Gilmore, and W. Gissler, *Surface and Coatings Technology*, Vol. 120-121, 1999, pp. 453-457
- [40] J. Robertson, *Materials Science and Engineering R*, Vol. 271, 2002, pp. 1-153